Robust treatment of cross points in Optimized Schwarz Methods

Xavier Claeys, Emile Parolin

Robust treatment of cross-points in Optimized Schwarz Methods

Xavier Claeys · Emile Parolin

Abstract In the field of Domain Decomposition (DD), Optimized Schwarz Method (OSM) appears to be one of the prominent techniques to solve large scale time-harmonic wave propagation problems. It is based on appropriate transmission conditions using carefully designed impedance operators to exchange information between subdomains. The efficiency of such methods is however hindered by the presence of cross-points, where more than two subdomains abut, if no appropriate treatment is provided.

In this work, we propose a new treatment of the cross-point issue for the Helmholtz equation that remains valid in any geometrical interface configuration. We exploit the multi-trace formalism to define a new exchange operator with suitable continuity and isometry properties. We then develop a complete theoretical framework that generalizes classical OSM to partitions with cross-points and contains a rigorous proof of geometric convergence, uniform with respect to the mesh discretization, for appropriate positive impedance operators. Extensive numerical results in 2D and 3D are provided as an illustration of the proposed method.

Keywords domain decomposition · optimized Schwarz methods · cross-points · acoustics

Mathematics Subject Classification (2010) 65N55 · 65F10 · 65N22

Introduction

Domain Decomposition (DD) for time-harmonic wave propagation is presently an active field of research as the numerical simulation of large scale problems remains a challenge in scientific computing. The additional difficulty of such problems, in

X. Claeys
Sorbonne Université, Université Paris-Diderot SPC, CNRS, Inria, Laboratoire Jacques-Louis Lions, équipe Alpines
E-mail: claeys@ljll.math.upmc.fr

E. Parolin
POems, UMR CNRS/ENSTA/Inria, Institut Polytechnique de Paris
E-mail: emile.parolin@inria.fr

comparison to elliptic problems, mainly lies in the (a priori) indefiniteness of the Helmholtz equation and related linear systems after discretization. In this work, we are interested in the sub-class of so-called (non-overlapping) Optimized Schwarz Methods (OSM) that appear as the most established approach in a wave context. In the context of waves, OSM dates back to the PhD thesis of Després [14,15, 16,17] where the idea to use Robin or impedance like transmission quantities was first introduced and a proof of algebraic convergence using energy estimates was derived. Many refinements over this initial idea were proposed since then in order to improve the rate of convergence exhibited. Most of the methods that were latter derived rely on the definition of a generalized Robin quantity with the introduction of an impedance operator. In this spirit, second order impedance operators (which possess sufficient properties for guaranteed convergence) were introduced by Gander, Magoulès and Nataf [23] and detailed in later works [25,34]. A popular approach was then developed which consists in using a (high-order) absorbing boundary condition (ABC) as transmission condition. The underlying idea is to approximate the Dirichlet-to-Neumann (DtN) map in the complementary domain, which provides exact transparent conditions albeit at a prohibitive numerical cost. This is the approach adopted in [4,20] for instance where Padé-approximants of the square root operator are used to construct high-order ABC. However, despite their efficiency in practice, such methods lack a rigorous analysis of convergence since only partial proofs in specific geometries are available. Another alternative, advocated in [12,13,32], is to use suitable non-local operators, realized in practice with integral operators, as impedance operators. One of the strengths of this later approach is to rely on a solid theoretical basis that systematically guarantees (h-uniform [9]) geometric convergence, provided that certain properties of injectivity, surjectivity and positivity (in suitable trace spaces) are satisfied by the impedance operator.

For realistic large scale applications, DD methods should be applicable to domain partitions with cross-points, where at least three subdomains share a common vertex. The presence of such points can be an issue both for the analysis at the continuous level and in practice for numerical implementations. For DD methods used in conjunction with zeroth order transmission operators, the convergence proof is established at the continuous level and in the case of mixed finite element discretizations, for instance in [16]. Interestingly, this particular choice of discretization avoids degrees of freedom (DOF) at cross-points and therefore the issue altogether. In contrast, the cross-point issue arises if one makes the choice of using nodal finite element discretizations, see [33,41]. Gander and Kwok [22] pointed that straightforward nodal discretization of OSM can diverge and that the continuous proof (based on Lions' energy estimates) fails to carry over to the discrete setting in general. Dual-Primal treatment of the problem at the discrete level has been developed which introduces additional global unknowns at cross-points effectively coupling all subdomains [1,2]. This leads to a global indefinite system that needs to be solved at each iteration. As regards the continuous theory available for DD methods constructed using non-local operators [12,13,32], it rests unfortunately on the strong hypothesis of the absence of cross-points between interfaces [32, Rem. 3]. Analysis suggests that this issue is related to the exchange operator being not continuous in proper trace norms in the presence of cross-points. Recently, the cross-point problem has been addressed by Després, Nicolopoulos and Thierry [18] for a particular class of second-order transmission

operators for which convergence of iterative algorithms is proven by using energy estimate techniques, though without any estimation of the convergence rate. Besides, Modave *et al* [36] presented a treatment of cross-points in the context of high-order ABC based transmission conditions. This later approach is however only valid on Cartesian like partitions of the mesh, allowing only cross-points where exactly four domains abut (in 2D), and no convergence theory is provided. It is clear that being able to deal with more general partitions, generated for instance by graph partitioners, is a highly desirable property.

The goal of this work is to use the clean treatment of cross-points from the Multi-Trace (MTF) formalism [10], initially developed for boundary integral equations (BIE), to investigate OSM. The main idea is to introduce a regularized version of the exchange operator, that remains isometric and continuous regardless of cross-points. The starting point is to recognize that if one uses positive impedance operators in the DD algorithm, it is possible to define a scalar product on the multi-trace space (collection of traces of local solutions in the subdomains). We then use this scalar product to define an orthogonal projector onto the single-trace space (collection of traces that match across interfaces), which is a closed subspace of the multi-trace space, in a very natural way. This provides a discrete characterization of the continuity of both the Dirichlet and Neumann traces across interfaces, that remains valid in the presence of cross-points. The definition of the exchange operator exploits this characterization using orthogonal projection and can be realized in practice by solving a positive linear system posed on the skeleton of the partition. As a result, since its computation amounts to solving a linear system, the exchange operator is *a priori* non-local. However, the structure of the auxiliary problem and in particular its definiteness are propitious to an efficient inversion, even in a distributed-memory parallelization context. Closely related ideas have been developed in a previous work [8] by the first author, at the continuous level. In contrast to this work, the exchange operator was there defined explicitly in terms of boundary integral operators.

Having defined this new way of exchanging traces across interfaces, the classical DD algorithms remain unchanged and the coupled local systems can be equivalently recast as a problem posed on the skeleton as usual. In fact, in the absence of cross-point, our approach reduces to traditional OSM so that our work can be seen as a generalization of previously described methods. The continuity and isometric properties of the exchange operator together with the contractivity of the local scattering operators yield immediately geometric convergence of the Richardson algorithm, despite the presence of cross-points. We show that in the case of geometric partitioning independent of the triangulation, using uniformly bounded impedance operators with respect to mesh discretization allows to obtain a uniform convergence rate.

The present contribution describes what we believe is the first DDM substructuring strategy for waves with guaranteed geometric convergence regardless of the presence of cross-points. We also provide a theoretical framework that applies in general geometric configurations while previous theoretical contributions on OSM either discarded the presence of cross-points [12, 13, 32], proposed a convergence result with no estimate of the convergence rate [16], or considered positive definite problems [24, 33, 37]. When there is no cross-point, and for a proper choice of impedance, the DDM approach presented here coincides with the method of

Després [14,15,16,17] and, as a byproduct, our analysis also provides new convergence estimates for Després algorithm, see Example 11.4.

Although derivation of high frequency robust numerical strategies is not the primary focus of the present contribution, our analysis remains valid in the high frequency regime. This does not mean that our method enjoys a frequency uniform convergence rate. However Proposition 10.4 establishes a link between the discrete inf-sup condition of the initial wave propagation problem and the convergence rate of our DDM strategy and, under the minimal assumption that the initial finite element matrix is invertible, this correspondence holds independently of the frequency regime and the mesh width parameter.

This article is organized as follows. In Section 1 we shortly describe the problem under consideration, before describing the geometric partitioning in Section 2 and an adapted functional framework in Section 3 and 4. The definitions of impedance operators and associated scalar products are then given in Section 5. In Section 6, the essential Lemma 6.2 states the properties of the exchange operator and the discrete characterization of the continuity of Dirichlet and Neumann traces. Section 8 recasts the problem at interfaces and proves that the equivalent problem and the local sub-problems are well posed. Section 9 describes the usual Richardson algorithm of our DD method and Theorem 9.2 states that one obtains geometric convergence of the iterative solution towards the solution of the original model problem. Section 10 on discrete stability gives an explicit lower bound for the inf-sup constant associated to the problem on the skeleton. This result yields uniform rate of convergence of iterative algorithms with respect to the mesh discretization, in the particular case of uniformly bounded impedance operators, as stated in Corollary 11.3, Section 11. We show how the proposed method is a generalization of classical OSM in Section 12. The algorithm in matrix form is detailed in Section 13, before extensive numerical results are reported in Section 14. We provide iteration counts for the Richardson and GMRes algorithms in 2D and 3D configurations with cross-points with physical boundaries as well as interior cross-points. The influence of several impedance operators with respect to different parameters: typical mesh size, wave number, number of subdomains and varying coefficients (heterogeneous medium) is studied.

1 Problem under study

We consider a very classical boundary value problem modeling scalar wave propagation in an *a priori* heterogeneous medium in $\mathbb{R}^d$ with $d = 1, 2$ or 3. The computational domain $\Omega \subset \mathbb{R}^d$ will be assumed bounded and polygonal ($d = 2$) or polyhedral ($d = 3$) for the sake of simplicity. The material characteristics of the propagation medium will be represented by two functions satisfying the following assumptions.

Assumption 1.1
The functions $\kappa : \Omega \to \mathbb{C}$ and $\mu : \Omega \to (0, +\infty)$ are measurable and satisfy

(i) $\Im\mathrm{m}\{\kappa(\boldsymbol{x})\} \geq 0, \Re\mathrm{e}\{\kappa(\boldsymbol{x})\} \geq 0 \; \forall \boldsymbol{x} \in \Omega$
(ii) $\kappa_\infty := \max(1, \|\kappa\|_{\mathrm{L}^\infty(\Omega)}) < +\infty$
(iii) $\|\mu\|_{\mathrm{L}^\infty(\Omega)} + \|\mu^{-1}\|_{\mathrm{L}^\infty(\Omega)} < +\infty.$

These are both general and physically reasonable assumptions. Condition *(i)* above implies in particular that $\Im\mathrm{m}\{\kappa^2(\boldsymbol{x})\} \geq 0$ and $\Im\mathrm{m}\{i\kappa(\boldsymbol{x})\} \geq 0$ for all $\boldsymbol{x} \in \Omega$. This means that the medium can only absorb or propagate energy. The above assumptions cover the case of discontinuous material coefficients - piecewise constants for example. In addition, we consider source terms $f \in \mathrm{L}^2(\Omega)$ and $g \in \mathrm{L}^2(\partial\Omega)$. The boundary value problem under consideration will be

$$\begin{cases} \text{Find } u \in \mathrm{H}^1(\Omega) \text{ such that} \\ -\operatorname{div}(\mu\nabla u) - \kappa^2 u = f \quad \text{in } \Omega, \\ (\mu\partial_{\boldsymbol{n}} - i\kappa)\, u = g \quad \text{on } \partial\Omega. \end{cases} \tag{1}$$

where $\boldsymbol{n}$ refers to the outward unit normal vector to $\partial\Omega$. As usual, for any domain $\omega \subset \Omega$, we consider the Sobolev space $\mathrm{H}^1(\omega) := \{v \in \mathrm{L}^2(\omega) : \nabla v \in \mathrm{L}^2(\omega)\}$, and the space of Dirichlet traces $\mathrm{H}^{1/2}(\partial\omega) := \{v|_{\partial\omega} : \ v \in \mathrm{H}^1(\omega)\}$. Because we are considering a wave propagation problem, inspired by [27], we shall equip those two spaces with the following norms

$$\begin{aligned} \|v\|^2_{\mathrm{H}^1(\omega)} &:= \|\nabla v\|^2_{\mathrm{L}^2(\omega)} + \kappa^2_\infty \|v\|^2_{\mathrm{L}^2(\omega)}, \\ \|q\|_{\mathrm{H}^{1/2}(\partial\omega)} &:= \min\{\|v\|_{\mathrm{H}^1(\omega)} : v \in \mathrm{H}^1(\omega), v|_{\partial\omega} = q\}. \end{aligned} \tag{2}$$

These norms involve some dependency with respect to the wave number κ which appears as an appropriate setting to derive frequency uniform results, see e.g. [35]. As usual, Problem (1) can be put in variational form: Find $u \in \mathrm{H}^1(\Omega)$ such that $a(u, v) = \ell(v)\ \forall v \in \mathrm{H}^1(\Omega)$ where

$$\begin{aligned} a(u, v) &:= \textstyle\int_\Omega \mu\nabla u \cdot \nabla\overline{v} - \kappa^2 u\overline{v}\, \mathrm{d}\boldsymbol{x} \ - i\int_{\partial\Omega} \kappa u\overline{v}\, \mathrm{d}\sigma \\ \ell(v) &:= \textstyle\int_\Omega f\overline{v}\, \mathrm{d}\boldsymbol{x} + \int_{\partial\Omega} g\overline{v}\, \mathrm{d}\sigma \end{aligned} \tag{3}$$

We are particularly interested in an effective numerical solution to (1), so we assume given a regular simplicial triangulation $\mathcal{T}_h(\Omega)$ of the domain Ω, and we assume $\overline{\Omega} = \cup_{\tau\in\mathcal{T}_h(\Omega)}\overline{\tau}$. We shall denote $\mathrm{V}_h(\Omega) \subset \mathrm{H}^1(\Omega)$ the space generated by conforming $\mathbb{P}_k$-Lagrange functions ($k \geq 1$) constructed on $\mathcal{T}_h(\Omega)$ [21],

$$\mathrm{V}_h(\Omega) := \{v_h \in \mathscr{C}^0(\overline{\Omega}) : \ v_h|_\tau \in \mathbb{P}_k(\tau), \forall\tau \in \mathcal{T}_h(\Omega)\}.$$

If $\omega \subset \Omega$ is any open subset that is resolved by the triangulation i.e. $\overline{\omega} = \cup_{\tau\in\mathcal{T}_h(\omega)}\overline{\tau}$, where $\mathcal{T}_h(\omega) := \{\tau \in \mathcal{T}_h(\Omega) : \tau \subset \overline{\omega}\}$, then we denote $\mathrm{V}_h(\omega) := \{\varphi|_\omega : \ \varphi \in \mathrm{V}_h(\Omega)\}$ and $\mathrm{V}_h(\partial\omega) := \{\varphi|_{\partial\omega} : \ \varphi \in \mathrm{V}_h(\Omega)\}$. We will focus on the discrete variational formulation

$$\begin{aligned} &\text{Find } u_h \in \mathrm{V}_h(\Omega) \text{ such that} \\ &a(u_h, v_h) = \ell(v_h) \quad \forall v_h \in \mathrm{V}_h(\Omega). \end{aligned} \tag{4}$$

Devising efficient domain decomposition algorithms to solve this discrete problem is the main goal of the present article. We make the general assumption that the material characteristics and the mesh width are chosen so as to guarantee unique solvability of the discrete problem.

Assumption 1.2

$$\alpha_h := \inf_{u\in\mathrm{V}_h(\Omega)\setminus\{0\}} \sup_{v\in\mathrm{V}_h(\Omega)\setminus\{0\}} \frac{|a(u,v)|}{\|u\|_{\mathrm{H}^1(\Omega)}\|v\|_{\mathrm{H}^1(\Omega)}} > 0.$$

This assumption simply means that the finite element matrix associated to (4) is invertible. This is a reasonable assumption and hardly any numerical analysis seems possible without it. As a consequence, in the remaining of this article, we shall systematically assume $\alpha_h > 0$.

Remark 1.3 *In the general case, there is a mesh-threshold $\overline{h} > 0$ such that $\alpha_h > 0$ for $h \in (0, \overline{h})$. The mesh-threshold is a function that depends on the material characteristics and the geometry $\overline{h} = \overline{h}(\kappa, \mu, \Omega)$ so Assumption 1.2 should be understood as a condition imposed on h, μ, κ, Ω all together; this is not just a condition on h alone.*

Remark 1.4 *For fixed material characteristics μ, κ and fixed geometry Ω, it is a classical consequence of Lax-Milgram's and Cea's lemma (see e.g. [30, chap.2]) that unique solvability of Problem* (1) *implies unique solvability of* (4) *for a sufficiently fine mesh, and that the sesquilinear form $a(\cdot, \cdot)$ satisfies a uniform discrete lower bound $\alpha_\star := \liminf_{h \to 0} \alpha_h > 0$.*

2 Geometric partitioning

We wish to describe and analyze a particular strategy for the solution of Problem (4) based on domain decomposition. As a consequence we assume that the computational domain admits the decomposition

$$\begin{aligned} &\overline{\Omega} = \cup_{j=1}^{\mathrm{J}} \overline{\Omega}_j^h, \text{ with } \quad \Omega_j^h \cap \Omega_k^h = \emptyset \quad \text{for } j \neq k \\ &\Sigma := \cup_{j=1}^{\mathrm{J}} \Gamma_j^h, \text{ where } \quad \Gamma_j^h := \partial \Omega_j^h, \end{aligned} \tag{5}$$

where each $\Omega_j^h \subset \Omega$ is itself a polyhedral domain that is exactly resolved by the triangulation. Figure 1 below gives examples of the type of triangulation we consider.

A typical situation occurs when the computational domain is decomposed as a first step in subdomains and, only afterwards, the mesh is generated in each subdomain separately. In this case, mesh-conformity between subdomain triangulations has to be enforced at interfaces. An example of this situation is represented in Figure 1a. Each subdomain Ω_j^h, and the subdomain partition itself, then remains unchanged as $h \to 0$. This is the case when the following condition is satisfied.

Condition 2.1 (fixed partition)
The subdomains $\Omega_j^h = \Omega_j$, $j = 1, \dots, \mathrm{J}$ are independent of the triangulation $\mathcal{T}_h(\Omega)$.

However, we will *not* consider that Condition 2.1 holds in general (except in the examples of Section 5 and in Section 11), because this partitioning approach is not the most convenient from a practical viewpoint. This is the reason why we refer to it as a "condition" instead of an "assumption".

Another approach consists in generating a mesh on the whole computational domain Ω first, and then subdividing it in subdomains by means of a graph partitioner such as e.g. Metis [31]. In this manner, conformity of subdomain triangulations at interfaces is automatically satisfied. However the partition itself has no

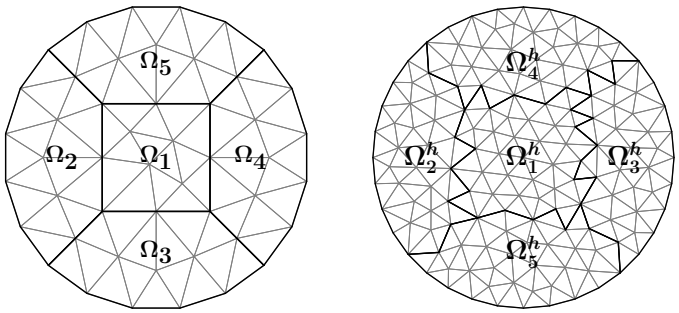

(a) (b)

Fig. 1: Two approaches for partitioning the computational domain.

reason to stabilize for $h \to 0$, and there is no guarantee that the geometry of each subdomain converges. Boundaries of subdomains may get rougher as $h \to 0$. This second situation is depicted in Figure 1b.

The analysis we present here covers both situations (a) and (b). Our geometrical setting allows the presence of cross-points on the skeleton Σ i.e. points where at least three subdomains may be adjacent. Because each Ω_j^h is resolved by the triangulation, so is each boundary Γ_j^h as well as the skeleton Σ.

3 Multi-domain functional setting

We introduce continuous and discrete function spaces naturally associated to this multi-domain setting. First we define $\mathbb{H}^1(\Omega) := \{u \in \mathrm{L}^2(\Omega) : \ u|_{\Omega_j^h} \in \mathrm{H}^1(\Omega_j^h) \ \forall j\}$ which contains the usual Sobolev space $\mathrm{H}^1(\Omega) \subset \mathbb{H}^1(\Omega)$. Next we consider the associated finite element spaces

$$\begin{aligned} &\mathbb{V}_h(\Omega) := \{u \in \mathrm{L}^2(\Omega) : \ u|_{\Omega_j^h} \in \mathrm{V}_h(\Omega_j^h) \ \forall j\} \ \subset \ \mathbb{H}^1(\Omega) \\ &\text{so that } \ \mathrm{V}_h(\Omega) = \mathrm{H}^1(\Omega) \cap \mathbb{V}_h(\Omega) \subset \mathbb{V}_h(\Omega). \end{aligned} \tag{6}$$

The space $\mathbb{V}_h(\Omega)$ consists in functions that are $\mathbb{P}_1$-Lagrange piecewise with respect to the subdomain partition. It is naturally isomorphic to $\mathrm{V}_h(\Omega_1) \times \cdots \times \mathrm{V}_h(\Omega_\mathrm{J})$. The elements of $\mathbb{V}_h(\Omega)$ may possibly admit Dirichlet jumps across interfaces between subdomains, while $\mathrm{V}_h(\Omega)$ is a closed subspace of $\mathbb{V}_h(\Omega)$ characterized by the constraint that Dirichlet traces match across interfaces $\Gamma_j^h \cap \Gamma_k^h$. Since we will be interested in transmission conditions, we need to consider the trace operation

$$v|_\Sigma := (v|_{\Gamma_1^h}, \ldots, v|_{\Gamma_\mathrm{J}^h})$$

where each $v|_{\Gamma_j^h}$ is a Dirichlet trace taken *from the interior* of the subdomain Ω_j^h, which is a convention we will systematically adopt through this article. The trace operator above continuously maps $\mathbb{V}_h(\Omega)$ (resp. $\mathrm{V}_h(\Omega)$) onto the space of Dirichlet multi-traces (resp. single-traces)

$$\begin{aligned} &\mathbb{V}_h(\Sigma) := \{v|_\Sigma : \ v \in \mathbb{V}_h(\Omega)\} = \mathrm{V}_h(\Gamma_1^h) \times \cdots \times \mathrm{V}_h(\Gamma_\mathrm{J}^h) \\ &\mathrm{V}_h(\Sigma) := \{v|_\Sigma : \ v \in \mathrm{V}_h(\Omega)\} \subset \mathbb{V}_h(\Sigma). \end{aligned} \tag{7}$$

where $\mathrm{V}_h(\Gamma_j^h) = \{v|_{\Gamma_j^h} : v \in \mathrm{V}_h(\Omega)\}$, see Section 1. In notations (6)-(7), we used the letter "$\mathbb{V}$" for reference to spaces where no continuity constraint is imposed at interfaces, and we used the letter "V" for reference to spaces where continuity holds through interfaces. The spaces $\mathbb{V}_h(\Omega)$ and $\mathbb{V}_h(\Sigma)$ are naturally equipped with cartesian product norms stemming from (2): for $u \in \mathbb{V}_h(\Omega)$ and $\mathfrak{q} = (q_1, \dots, q_\mathrm{J}) \in \mathbb{V}_h(\Sigma)$ we set

$$\begin{aligned} \|u\|^2_{\mathbb{H}^1(\Omega)} &:= \|u|_{\Omega_1^h}\|^2_{\mathrm{H}^1(\Omega_1^h)} + \cdots + \|u|_{\Omega_\mathrm{J}^h}\|^2_{\mathrm{H}^1(\Omega_\mathrm{J}^h)}, \\ \|\mathfrak{q}\|^2_{\mathbb{H}^{1/2}(\Sigma)} &:= \|q_1\|^2_{\mathrm{H}^{1/2}(\Gamma_1^h)} + \cdots + \|q_\mathrm{J}\|^2_{\mathrm{H}^{1/2}(\Gamma_\mathrm{J}^h)}. \end{aligned} \tag{8}$$

4 Discrete harmonic extensions

Besides (8), several choices of norms are possible for the multi-trace space $\mathbb{V}_h(\Sigma) = \mathrm{V}_h(\Gamma_1^h) \times \cdots \times \mathrm{V}_h(\Gamma_\mathrm{J}^h)$. Because we are dealing with a discrete variational formulation, there is another norm, of a more discrete nature, that will arise as pivotal in our analysis. To describe it, we first introduce norm minimizing lifting operators $\rho_j : \mathrm{V}_h(\Gamma_j^h) \to \mathrm{V}_h(\Omega_j^h)$ defined, for all $q \in \mathrm{V}_h(\Gamma_j^h)$, by

$$\begin{aligned} &\rho_j(q) \in \mathrm{V}_h(\Omega_j^h),\ \rho_j(q)|_{\Gamma_j^h} = q \ \text{ and} \\ &\|\rho_j(q)\|_{\mathrm{H}^1(\Omega_j^h)} = \min\{\|v\|_{\mathrm{H}^1(\Omega_j^h)} :\ v \in \mathrm{V}_h(\Omega_j^h), v|_{\Gamma_j^h} = q\}. \end{aligned} \tag{9}$$

Such operators are commonly encountered in domain decomposition literature (see e.g. [43, §4.4] or [37, 1.2.6]) and are sometimes referred to as harmonic extension maps. These can be collected into a global lifting operator defined by

$$\begin{aligned} &\rho_h : \mathbb{V}_h(\Sigma) \to \mathbb{V}_h(\Omega), \\ &\rho_h(\mathfrak{q})|_{\Omega_j} := \rho_j(q_j) \ \ \forall j = 1 \dots \mathrm{J} \end{aligned}$$

for all $\mathfrak{q} = (q_1, \dots, q_\mathrm{J})$. By construction we have $\rho_h(\mathfrak{q})|_\Sigma = \mathfrak{q}$ and, in particular, ρ_h is one-to-one. A possible norm for discrete Dirichlet traces stems directly from discrete harmonic extension maps. For $\mathfrak{q} = (q_1, \dots, q_\mathrm{J}) \in \mathbb{V}_h(\Sigma)$ we set

$$\|\mathfrak{q}\|^2_{\rho_h} := \|\rho_h(\mathfrak{q})\|^2_{\mathbb{H}^1(\Omega)} := \sum_{j=1}^{\mathrm{J}} \|\rho_j(q_j)\|^2_{\mathrm{H}^1(\Omega_j^h)}. \tag{10}$$

By the very definition of this norm, the operator ρ_h has unitary continuity modulus. The norm (10) inherits wave number dependency from (2). It also a priori depends on the triangulation because minimization in (9) is performed over the discrete space $\mathrm{V}_h(\Omega_j^h)$.

Comparing (9)-(10) on one hand, and (2)-(8) on the other hand, the norm $\|\cdot\|_{\rho_h}$ appears as a discrete counterpart of $\|\cdot\|_{\mathbb{H}^{1/2}(\Sigma)}$. For fixed material characteristics these two norms are actually h-uniformly equivalent.

Lemma 4.1
The continuity of the trace operator systematically implies $\|\mathfrak{q}\|_{\mathbb{H}^{1/2}(\Sigma)} \leq \|\mathfrak{q}\|_{\rho_h}$ *for*

all $\mathfrak{q} \in \mathbb{V}_h(\Sigma)$. *Assume in addition that the family of triangulations* $\{\mathcal{T}_h(\Omega)\}_{h>0}$ *is h-uniformly shape regular,*

$$\liminf_{h\to 0,\tau\in\mathcal{T}_h(\Omega)} \sup\{\mathrm{diam(B)} :\ \mathrm{B}\ \textit{is a ball} \subset \tau\}/\mathrm{diam}(\tau) > 0 \tag{11}$$

and that the material characteristics (in particular the wave number) are fixed as well as the computational domain Ω. *Then the discrete harmonic extension operator is h-uniformly bounded*

$$\limsup_{h\to 0} \sup_{\mathfrak{q}\in\mathbb{V}_h(\Sigma)\setminus\{0\}} \frac{\|\mathfrak{q}\|_{\rho_h}}{\|\mathfrak{q}\|_{\mathbb{H}^{\frac{1}{2}}(\Sigma)}} < +\infty.$$

Proof:

For any $p \in \mathrm{H}^{1/2}(\Gamma_j^h)$ define $\theta_j(p)$ as the unique element of $\mathrm{H}^1(\Omega_j^h)$ satisfying $\theta_j(p)|_{\Gamma_j^h} = p$ and $\|\theta_j(p)\|_{\mathrm{H}^1(\Omega_j^h)} = \min\{\|v\|_{\mathrm{H}^1(\Omega_j^h)} :\ v \in \mathrm{H}^1(\Omega_j^h),\ v|_{\Gamma_j^h} = p\}$, and then define $\theta : \mathbb{H}^{1/2}(\Sigma) \to \mathbb{H}^1(\Omega)$ by $\theta(q_1,\ldots,q_J)|_{\Omega_j^h} := \theta_j(q_j)$ for all $j = 1\ldots \mathrm{J}$. Here the operator θ is similar to the operator ρ_h in the sense that it is also an harmonic extension map, but defined on the continuous spaces. By definition of the norms (2)-(8) we have for any $\mathfrak{q} \in \mathbb{H}^{1/2}(\Sigma)$

$$\|\mathfrak{q}\|_{\mathbb{H}^{1/2}(\Sigma)} = \|\theta(\mathfrak{q})\|_{\mathbb{H}^1(\Omega)}. \tag{12}$$

Next let $\pi_{h,j} : \mathrm{H}^1(\Omega_j^h) \to \mathrm{V}_h(\Omega_j^h)$ refer to the Scott-Zhang interpolation operator [39] and [5, §4.8]. This operator satisfies $\pi_{h,j}(v) = v$ for all $v \in \mathrm{V}_h(\Omega_j^h)$, and it is uniformly bounded

$$\limsup_{h\to 0} \sup_{v\in\mathrm{H}^1(\Omega_j^h)\setminus\{0\}} \|\pi_{h,j}(v)\|_{\mathrm{H}^1(\Omega_j^h)}/\|v\|_{\mathrm{H}^1(\Omega_j^h)} < +\infty. \tag{13}$$

This modulus of the Scott-Zhang interpolator only depends on the shape regularity constant (11) of the triangulation and is thus bounded independently of the shape of the subdomains. Besides it can be defined in such a way that it guarantees $\pi_{j,h}(v)|_{\Gamma_j^h} = v|_{\Gamma_j^h}$ if $v|_{\Gamma_j^h} \in \mathrm{V}_h(\Gamma_j^h)$. Define $\pi_h : \mathbb{H}^1(\Omega) \to \mathbb{V}_h(\Omega)$ by collecting these local Scott-Zhang operators $\pi_h(v)|_{\Omega_j^h} := \pi_{j,h}(v|_{\Omega_j^h})$ for all $j = 1\ldots \mathrm{J}$. From (13) we deduce

$$C_\pi = \limsup_{h\to 0} \sup_{v\in\mathbb{H}^1(\Omega)\setminus\{0\}} \|\pi_h(v)\|_{\mathbb{H}^1(\Omega)}/\|v\|_{\mathbb{H}^1(\Omega)} < +\infty. \tag{14}$$

Finally, taking account of the definition of $\|\cdot\|_{\rho_h}$ given by (9)-(10), we obtain $\|\mathfrak{q}\|_{\rho_h} = \|\rho_h(\mathfrak{q})\|_{\mathbb{H}^1(\Omega)} \le \|\pi_h(\theta(\mathfrak{q}))\|_{\mathbb{H}^1(\Omega)} \le C_\pi\|\theta(\mathfrak{q})\|_{\mathbb{H}^1(\Omega)} = C_\pi\|\mathfrak{q}\|_{\mathbb{H}^{1/2}(\Sigma)}$ for any $\mathfrak{q} \in \mathbb{H}^{1/2}(\Sigma)$. □

To conclude this paragraph, let us point that the constant associated to the $\limsup_{h\to 0}$ in Lemma 4.1 above a priori depends on the material characteristics and in particular the wave number.

5 Impedance operator

To define a scalar product on the space of traces, one may of course consider the scalar product associated with (10) or (8). Many other choices are possible that appear more convenient in a finite element context. This is why we will *a priori* consider another one.

Assumption 5.1
The sesquilinear form $t_h(\cdot,\cdot) : \mathbb{V}_h(\Sigma) \times \mathbb{V}_h(\Sigma) \to \mathbb{C}$ is a scalar product, and the associated norm is denoted

$$\|\mathfrak{w}\|_{t_h} := \sqrt{t_h(\mathfrak{w},\mathfrak{w})}.$$

We state this as an assumption because the sesquilinear form $t_h(\cdot,\cdot)$, that we shall later refer to as the *impedance*, will play a central role in our theory, and it is important to underline that our analysis allows rather general form for the impedance.

We insist that no other assumption on the impedance is needed for the subsequent analysis. In particular we do not assume that $t_h(\cdot,\cdot)$ satisfies a uniform discrete inf-sup condition so that $\|\cdot\|_{t_h}$ need not be h-uniformly equivalent to $\|\cdot\|_{\mathbb{H}^{1/2}(\Sigma)}$ or $\|\cdot\|_{\rho_h}$. The following quantities will come into play

$$\lambda_h^- := \inf_{\mathfrak{w}\in\mathbb{V}_h(\Sigma)\setminus\{0\}} \frac{\|\mathfrak{w}\|_{t_h}}{\|\mathfrak{w}\|_{\rho_h}} \qquad \text{and} \qquad \lambda_h^+ := \sup_{\mathfrak{w}\in\mathbb{V}_h(\Sigma)\setminus\{0\}} \frac{\|\mathfrak{w}\|_{t_h}}{\|\mathfrak{w}\|_{\rho_h}}. \tag{15}$$

Because $t_h(\cdot,\cdot)$ is supposed to be a scalar product, we have $0 < \lambda_h^- \leq \lambda_h^+ < +\infty$ for each h. However, in certain cases of practical importance, one may have $\liminf_{h\to 0} \lambda_h^- = 0$ or $\limsup_{h\to 0} \lambda_h^+ = +\infty$. To fix ideas, we give a few examples of possible impedance operators.

Example 5.2 (Després impedance) *Consider a fixed parameter $\kappa_{\mathrm{R}} > 0$ that will serve as a reference wave number. A first possible choice consists in defining impedance using surface mass matrices as follows*

$$t_h(\mathfrak{p},\mathfrak{q}) = \sum_{j=1}^{\mathrm{J}} \int_{\Gamma_j} \kappa_{\mathrm{R}}\, p_j \overline{q}_j \,\mathrm{d}\sigma. \tag{16}$$

This choice of impedance was the one originally introduced in [14, 15, 16, 17].

It is a scalar product on $\mathbb{V}_h(\Sigma)$ that is h-uniformly bounded $\limsup_{h\to 0} \lambda_h^+ < +\infty$. If Condition 2.1 holds and material characteristics are fixed, it does not satisfy any h-uniform discrete inf-sup condition. Inverse estimates show that there exists a constant $C > 0$ independent of h such that $\lambda_h^- \geq C\sqrt{h}$, see e.g [43, Lemma 4.11].

Example 5.3 (Second order differential operator) *Consider two constants $a, b > 0$ that, in practice, are fitting parameters requiring calibration. Another choice of impedance is based on an order 2 surface differential operator and involves both mass and stiffness matrices*

$$t_h(\mathfrak{p},\mathfrak{q}) = \sum_{j=1}^{\mathrm{J}} \int_{\Gamma_j} a\nabla_{\Gamma_j} p_j \cdot \nabla_{\Gamma_j} \overline{q}_j + b\, p_j \overline{q}_j \,\mathrm{d}\sigma. \tag{17}$$

In the choice above, the operators ∇_{Γ_j} refer to surface gradients. Many variants of this condition can be considered. The coefficients a, b may vary from one subdomain to another i.e. $a = a_j$ (resp. $b = b_j$) on Γ_j. Also these coefficients may depend on the mesh width h and the wave number κ. Such a choice of impedance (or a variant of it) was considered e.g. in [23, 34, 25].

Impedance (17) *also yields a scalar product on $\mathbb{V}_h(\Sigma)$. If Condition 2.1 holds and material characteristics are fixed, it can be proved to be h-uniformly inf-sup stable $\liminf_{h\to 0} \lambda_h^- > 0$, but it is not h-uniformly bounded anymore. Once again inverse estimates yield the existence of $C > 0$ independent of h such that $\lambda_h^+ \leq C/\sqrt{h}$.*

Example 5.4 (Integral operator based impedance) *Another possibility is an impedance based on some integral operator. Consider parameters $a, \delta > 0$. The parameter δ would represent how localized the kernel is. To mimic the properties of the trace norm, one may consider an analytical expression based on the hypersingular operator see e.g. [38, §3.3.4] or [42, §6.5]. For problems posed in $\mathbb{R}^3$ this would correspond to*

$$t_h(\mathfrak{p},\mathfrak{q}) = \sum_{j=1}^{\mathrm{J}} \int_{\Gamma_j\times\Gamma_j} a\, \frac{\exp(-|\boldsymbol{x}-\boldsymbol{y}|/\delta)}{4\pi|\boldsymbol{x}-\boldsymbol{y}|} \big(\operatorname{curl}_{\Gamma_j} p_j(\boldsymbol{x}) \cdot \operatorname{curl}_{\Gamma_j} \overline{q}_j(\boldsymbol{y}) + \delta^{-2} \boldsymbol{n}_j(\boldsymbol{x}) \cdot \boldsymbol{n}_j(\boldsymbol{y})\, p_j(\boldsymbol{x}) \overline{q}_j(\boldsymbol{y}) \big)\, \mathrm{d}\sigma(\boldsymbol{x},\boldsymbol{y}), \tag{18}$$

where $\boldsymbol{n}_j(\boldsymbol{x})$ is the vector normal to Γ_j directed toward the exterior of Ω_j, and $\operatorname{curl}_{\Gamma_j} v(\boldsymbol{x}) := \boldsymbol{n}_j(\boldsymbol{x}) \times \nabla_{\Gamma_j} v(\boldsymbol{x})$ is the surface curl. Such a choice was considered in [13, 32], and a variant of it was proposed in [11] in the context of Maxwell's equations. As discussed in [32, §3.1.3], the motivation for considering non-local impedances such as (18) *is that this leads to h-uniform rate of convergence of the OSM algorithm, in contrast with local impedances such as* (16) *or* (17)*.*

Once again (18) *is a scalar product on $\mathbb{V}_h(\Sigma)$. Because* (18) *stems from an operator that is both bounded and coercive in the continuous trace space, if Condition 2.1 holds and material characteristics are fixed, then $0 < \liminf_{h\to 0} \lambda_h^- \leq \limsup_{h\to 0} \lambda_h^+ < +\infty$.*

Example 5.5 (Schur complement based impedance) *Another non-local operator is given by a Schur complement based impedance operator, which corresponds to the scalar product associated to the following norm:*

$$t_h(\mathfrak{p},\mathfrak{p}) = \|\mathfrak{p}\|_{\rho_h}^2 = \|\rho_h(\mathfrak{p})\|_{\mathbb{H}^1(\Omega)}^2 = \sum_{j=1}^{\mathrm{J}} \|\rho_j(p_j)\|_{\mathrm{H}^1(\Omega_j^h)}^2, \tag{19}$$

where $\mathfrak{p} = (p_1, \ldots, p_{\mathrm{J}}) \in \mathbb{V}_h(\Sigma)$. In practice, computing this scalar product involves computing the local solutions $\rho_j(p_j)$, see (9)*, which can be done in parallel using the same numerical scheme and mesh as for the solutions u_j of the propagative local sub-problems.*

From the definition of $\lambda_h^\pm$ given by (15) *we readily obtain $\lambda_h^\pm = 1$ in this case, which implies unconditional h-uniform stability for this choice of operator.*

In all the examples we gave above, the impedance does not couple distinct subdomains i.e. it takes the form of a sum of local contributions, which is rather natural in the context of domain decomposition.

Definition 5.6 (Diagonal impedance)
A scalar product $t_h(\cdot,\cdot) : \mathbb{V}_h(\Sigma) \times \mathbb{V}_h(\Sigma) \to \mathbb{C}$ will be called diagonal if there are local scalar products $t_h^j(\cdot,\cdot) : \mathrm{V}_h(\Gamma_j^h) \times \mathrm{V}_h(\Gamma_j^h) \to \mathbb{C}$ such that, for $\mathfrak{p} = (p_1, \dots, p_{\mathrm{J}})$ and $\mathfrak{q} = (q_1, \dots, q_{\mathrm{J}})$, we have

$$t_h(\mathfrak{p}, \mathfrak{q}) = t_h^1(p_1, q_1) + \cdots + t_h^{\mathrm{J}}(p_{\mathrm{J}}, q_{\mathrm{J}}).$$

Many other choices of impedance operator are possible, see e.g. [12,32]. We do not assume a priori that the impedance $t_h(\cdot,\cdot)$ is diagonal because this is not needed for the subsequent analysis. Later on though, we shall point the practical benefit of considering diagonal impedances, see Remark 9.1.

To conclude this section we point out that the scalar product $t_h(\cdot,\cdot)$ will be used to represent linear functionals associated to boundary terms.

Lemma 5.7
Under Assumption 5.1, assume that $\phi : \mathbb{V}_h(\Omega) \to \mathbb{C}$ is a linear form satisfying $\phi(w) = 0$ for all $w \in \mathbb{V}_h(\Omega)$ such that $w|_\Sigma = 0$. Then there exists a unique $\mathfrak{q} \in \mathbb{V}_h(\Sigma)$ such that $\phi(v) = t_h(v|_\Sigma, \mathfrak{q}) \forall v \in \mathbb{V}_h(\Omega)$.

Proof:
Since $w = \rho_h(v|_\Sigma) - v \in \mathbb{V}_h(\Omega)$ satisfies $w|_\Sigma = 0$ for all $v \in \mathbb{V}_h(\Omega)$, we deduce that $\phi(v) = \phi(\rho_h(v|_\Sigma))$ for all $v \in \mathbb{V}_h(\Omega)$. Since $t_h(\cdot,\cdot)$ is a scalar product on $\mathbb{V}_h(\Sigma)$, there exists a unique $\mathfrak{q} \in \mathbb{V}_h(\Sigma)$ such that $t_h(\mathfrak{p}, \mathfrak{q}) = \phi(\rho_h(\mathfrak{p})) \forall \mathfrak{p} \in \mathbb{V}_h(\Sigma)$ by Riesz representation. □

6 Characterization of interface conditions

Transmission conditions are critical in domain decomposition because this is what induces coupling between subdomains. In the present section, we will work out a new way to impose them.

In (4), Dirichlet transmission conditions are enforced by assuming that traces match across interfaces. Such conditions are encoded into the single-trace space introduced in (7),

$$\mathrm{V}_h(\Sigma) = \{(u|_{\Gamma_j^h})_{j=1}^{\mathrm{J}} \in \mathbb{V}_h(\Sigma) : \ u \in \mathrm{V}_h(\Omega)\}.$$

This space is a discrete counterpart of what has been referred to as "Dirichlet single-trace" space in the literature dedicated to Multi-Trace formalism, see [6,7, 10]. We first state a simple result that helps characterize $\mathrm{V}_h(\Omega)$ as a subspace of $\mathbb{V}_h(\Omega)$ by means of its traces on the skeleton.

Lemma 6.1
Any $u \in \mathbb{V}_h(\Omega)$ belongs to $\mathrm{V}_h(\Omega)$ if and only if $u|_\Sigma \in \mathrm{V}_h(\Sigma)$.

An easy consequence of the previous lemma is that $\rho_h(\mathfrak{q}) \in \mathrm{V}_h(\Omega)$ whenever $\mathfrak{q} \in \mathrm{V}_h(\Sigma)$. Because we are aiming at domain decomposition, we wish to decouple subdomains as much as possible, and thus eliminate any reference to $\mathrm{V}_h(\Sigma)$. This is our motivation in searching for characterizations of this space. The next result provides such a characterization by means of an "exchange operator" Π. Its proof is routine verification left to the reader.

Lemma 6.2 (Exchange operator)
Under Assumption 5.1, define $\Pi : \mathbb{V}_h(\Sigma) \to \mathbb{V}_h(\Sigma)$ *such that* $(\mathrm{Id} + \Pi)/2$ *is the orthogonal projector onto* $\mathrm{V}_h(\Sigma)$ *for the scalar product* t_h*. Then* Π *is an isometry, we have* $\Pi^2 = \mathrm{Id}$ *and* $\|\Pi(\mathfrak{u})\|_{t_h} = \|\mathfrak{u}\|_{t_h}$ *for all* $\mathfrak{u} \in \mathbb{V}_h(\Sigma)$*. Moreover for any pair* $(\mathfrak{u}, \mathfrak{q}) \in \mathbb{V}_h(\Sigma) \times \mathbb{V}_h(\Sigma)$ *we have*

$$(\mathfrak{u}, \mathfrak{q}) \in \mathrm{V}_h(\Sigma) \times \mathrm{V}_h(\Sigma)^\perp \quad \Longleftrightarrow \quad -\mathfrak{q} + i\mathfrak{u} = \Pi(\mathfrak{q} + i\mathfrak{u}). \tag{20}$$

Computing the action of the exchange operator through the operation $\mathfrak{p} \mapsto \Pi(\mathfrak{p})$ is non-trivial from an effective computational viewpoint. This can be achieved through an orthogonal projection onto the subspace $\mathrm{V}_h(\Sigma)$ which, variationally, rewrites as follows

$$\begin{aligned} &\Pi(\mathfrak{q}) := -\mathfrak{q} + 2\mathfrak{p} \quad \text{where } \mathfrak{p} \in \mathrm{V}_h(\Sigma) \text{ solves} \\ &t_h(\mathfrak{p}, \mathfrak{w}) = t_h(\mathfrak{q}, \mathfrak{w}) \quad \forall \mathfrak{w} \in \mathrm{V}_h(\Sigma). \end{aligned} \tag{21}$$

Of course this orthogonal projection requires solving a problem posed globally on the whole skeleton Σ. Here the choice of the scalar product t_h does matter: it should be chosen so that the orthogonal projection in (21) is easy to compute. This variational problem makes the operator Π a priori non-local. For certain choices of impedance, this exchange operator may couple distant subdomains that are not a priori adjacent. This will be a salient feature of our strategy, and a key difference in comparison with existing literature.

Remark 6.3 *Admittedly, this non-locality raises a computational difficulty. However the variational problem* (21) *is symmetric positive definite, and takes the very same form as the Schur complement systems encountered in the analysis of substructuring methods, see [43, §4.3], [37, §2.1] or [19, §6.4]. Current literature offers very efficient scalable two level DDM preconditioners for tackling such a problem as* (21)*, like e.g. the GenEO approach [40].*

7 Reformulation of the wave propagation problem

In the previous section we discussed in depth the effect of domain partitioning on our discrete functional setting. This led us to propose, in Section 6, a new way of imposing transmission conditions, see (20). We now apply the outcomes of this discussion to the discrete problem (4) under study. The sesquilinear form $a(\cdot,\cdot)$ introduced in (3) extends as a map $a(\cdot,\cdot) : \mathbb{V}_h(\Omega) \times \mathbb{V}_h(\Omega) \to \mathbb{C}$ defined by

$$\begin{aligned} a(u, v) &:= \textstyle\sum_{j=1}^{\mathrm{J}} a_{\Omega_j^h}(u, v) \quad \text{where} \\ a_{\Omega_j^h}(u, v) &:= \textstyle\int_{\Omega_j^h} \mu \nabla u \cdot \nabla \overline{v} - \kappa^2 u \overline{v} \, \mathrm{d}\boldsymbol{x} - i \int_{\partial\Omega_j^h \cap \partial\Omega} \kappa u \overline{v} \, \mathrm{d}\sigma. \end{aligned}$$

Note that Assumptions 1.1 imply $\Im m\{a(u,u)\} \leq 0 \ \forall u \in \mathbb{V}_h(\Omega)$. Besides the inf-sup constant α_h introduced in Assumption 1.2, the material characteristics μ, κ and the geometry of Ω enter our analysis through the continuity modulus

$$\|a\| := \sup_{u,v \in \mathbb{H}^1(\Omega)\setminus\{0\}} \frac{|a(u,v)|}{\|u\|_{\mathbb{H}^1(\Omega)} \|v\|_{\mathbb{H}^1(\Omega)}}. \tag{22}$$

Remark 7.1 *The same arguments as in [27, Lem.2.4], and in particular the multiplicative trace inequality from [29, last equation on p.41], show that* $\|a\|$ *is bounded uniformly with respect to* $\sup_\Omega |\kappa|$.

Like for $a(\cdot,\cdot)$, the functional $\ell(\cdot)$ induces a continuous map on $\mathbb{V}_h(\Omega)$ defined for all $v \in \mathbb{V}_h(\Omega)$ by

$$\begin{aligned}\ell(v) &:= \textstyle\sum_{j=1}^{\mathrm{J}} \ell_{\Omega_j^h}(v) \quad \text{where}\\ \ell_{\Omega_j^h}(v) &:= \textstyle\int_{\Omega_j^h} f\overline{v}\,\mathrm{d}\boldsymbol{x} + \int_{\partial\Omega_j^h\cap\partial\Omega} g\overline{v}\,\mathrm{d}\sigma.\end{aligned}$$

The previous notations combined with the impedance $t_h(\cdot,\cdot)$ introduced in Section 5 can be used to reformulate (4) as a saddle-point problem involving the space $\mathbb{V}_h(\Omega)$ instead of $\mathrm{V}_h(\Omega)$, and enforcing transmission conditions by means of Lagrange multipliers.

Proposition 7.2
Let Assumption 5.1 hold, and set $\mathrm{V}_h(\Sigma)^\perp := \{\mathfrak{u} \in \mathbb{V}_h(\Sigma) : \ t_h(\mathfrak{u},\mathfrak{v}) = 0\ \forall \mathfrak{v} \in \mathrm{V}_h(\Sigma)\}$. *If the function* $u \in \mathrm{V}_h(\Omega)$ *solves* (4), *then there exists* $\mathfrak{q} \in \mathrm{V}_h(\Sigma)^\perp$ *such that*

$$\begin{aligned}&(u,\mathfrak{q}) \in \mathbb{V}_h(\Omega)\times \mathrm{V}_h(\Sigma)^\perp \quad \textit{and}\\ &a(u,v) - t_h(\mathfrak{q}, v|_\Sigma) = \ell(v) \quad \forall v \in \mathbb{V}_h(\Omega),\\ &t_h(u|_\Sigma, \mathfrak{w}) = 0 \qquad\qquad \forall \mathfrak{w} \in \mathrm{V}_h(\Sigma)^\perp.\end{aligned} \tag{23}$$

Reciprocally if $(u,\mathfrak{q}) \in \mathbb{V}_h(\Omega)\times \mathrm{V}_h(\Sigma)^\perp$ *solves* (23), *then* $u \in \mathrm{V}_h(\Omega)$ *and it is the unique solution to Problem* (4).

Proof:

Assume first that $u \in \mathrm{V}_h(\Omega)$ solves (4). By definition we have $u|_\Sigma \in \mathrm{V}_h(\Sigma)$ so that $t_h(u|_\Sigma, \mathfrak{w}) = 0\ \forall \mathfrak{w} \in \mathrm{V}_h(\Sigma)^\perp$. In addition, applying Lemma 5.7 to the functional $\phi(v) := a(u,v) - \ell(v), v \in \mathbb{V}_h(\Omega)$, we deduce that there exists $\mathfrak{q} \in \mathbb{V}_h(\Sigma)$ such that $a(u,v) - \ell(v) = t_h(\mathfrak{q}, v|_\Sigma)\ \forall v \in \mathbb{V}_h(\Omega)$. Besides we have $\phi(v) = 0\ \forall v \in \mathrm{V}_h(\Omega)$ by hypothesis which rewrites $t_h(\mathfrak{q},\mathfrak{p}) = 0\ \forall \mathfrak{p} \in \mathrm{V}_h(\Sigma)$ hence $\mathfrak{q} \in \mathrm{V}_h(\Sigma)^\perp$. This proves (23).

Reciprocally assume that (23) holds. According to Lemma 6.1, the second equation of (23) implies that $u \in \mathrm{V}_h(\Omega)$. Next, taking $v \in \mathrm{V}_h(\Omega)$ in the first equation (23) leads to $a(u,v) = \ell(v)$ for all $v \in \mathrm{V}_h(\Omega)$, which is (4). In conclusion u solves (4). □

The second equation of (23) simply re-writes $u|_\Sigma \in \mathrm{V}_h(\Sigma)$. In this saddle point problem, the transmission conditions stemming from the original problem (4) are encoded in the two conditions $u|_\Sigma \in \mathrm{V}_h(\Sigma)$ (Dirichlet transmission condition) and $\mathfrak{q} \in \mathrm{V}_h(\Sigma)^\perp$ (Neumann transmission condition), and (23) holds if and only if $(u,\mathfrak{q}) \in \mathbb{V}_h(\Omega)\times\mathbb{V}_h(\Sigma)$ satisfies $a(u,v) - t_h(\mathfrak{q}, v|_\Sigma) = \ell(v)\ \forall v \in \mathbb{V}_h(\Omega)$ and $(u|_\Sigma, \mathfrak{q}) \in \mathrm{V}_h(\Sigma)\times\mathrm{V}_h(\Sigma)^\perp$.

A key novelty of our analysis consists in using (20) to reformulate the two conditions $(u|_\Sigma, \mathfrak{q}) \in \mathrm{V}_h(\Sigma)\times\mathrm{V}_h(\Sigma)^\perp$ equivalently as $-\mathfrak{q} + iu|_\Sigma = \Pi(\mathfrak{q} + iu|_\Sigma)$. As a consequence $(u,\mathfrak{q})$ solves (23) if and only if it satisfies

$$\begin{aligned}&(u,\mathfrak{q}) \in \mathbb{V}_h(\Omega)\times\mathbb{V}_h(\Sigma) \ \text{ and}\\ &a(u,v) - t_h(\mathfrak{q}, v|_\Sigma) = \ell(v) \quad \forall v \in \mathbb{V}_h(\Omega),\\ &\mathfrak{q} - iu|_\Sigma = -\Pi(\mathfrak{q} + iu|_\Sigma).\end{aligned} \tag{24}$$

When it is considered on $\mathbb{V}_h(\Omega) \times \mathbb{V}_h(\Omega)$, the sesquilinear form $a(\cdot,\cdot)$ does not systematically satisfy an inf-sup condition. It may admit a non-trivial kernel in certain interior subdomains, which would be an artefact stemming from domain partitioning only. This is not satisfactory, and this motivates a change of unknowns $\mathfrak{p} = \mathfrak{q} - iu|_\Sigma$ which leads to another equivalent formulation of our problem.

Lemma 7.3
Under Assumption 5.1, if $u \in \mathrm{V}_h(\Omega)$ solves (4) then there exists a tuple of traces $\mathfrak{p} \in \mathbb{V}_h(\Sigma)$ such that

$$\begin{aligned} &(u,\mathfrak{p}) \in \mathbb{V}_h(\Omega) \times \mathbb{V}_h(\Sigma) \ \textit{and} \\ &\textit{(i)} \quad a(u,v) - it_h(u|_\Sigma, v|_\Sigma) = t_h(\mathfrak{p}, v|_\Sigma) + \ell(v) \quad \forall v \in \mathbb{V}_h(\Omega), \\ &\textit{(ii)} \quad \mathfrak{p} = -\Pi(\mathfrak{p} + 2iu|_\Sigma). \end{aligned} \tag{25}$$

Reciprocally if $(u,\mathfrak{p}) \in \mathbb{V}_h(\Omega) \times \mathbb{V}_h(\Sigma)$ solves (25), then $u \in \mathrm{V}_h(\Omega)$ and it is the unique solution to Problem (4), and $\mathfrak{p} + iu|_\Sigma \in \mathrm{V}_h(\Sigma)^\perp$ and the pair $(u,\mathfrak{q}) = (u, \mathfrak{p} + iu|_\Sigma)$ solves (23).

Formulation (25) plays a central role in the DDM strategy of the present contribution. It contains a volume part (i) which expresses wave equations in each subdomain, and a skeleton part (ii) that enforces transmission conditions and a (potentially non-local) coupling between subdomains. Due to the positivity properties of t_h, the sesquilinear form $u, v \mapsto a(u,v) - it_h(u|_\Sigma, v|_\Sigma)$ satisfies an inf-sup condition.

Lemma 7.4 (Well posedness of local sub-problems)
Under Assumptions 1.1, 1.2 and 5.1 we have

$$\beta_h := \inf_{u \in \mathbb{V}_h(\Omega)\setminus\{0\}} \sup_{v \in \mathbb{V}_h(\Omega)\setminus\{0\}} \frac{|\, a(u,v) - it_h(u|_\Sigma, v|_\Sigma)\,|}{\|u\|_{\mathbb{H}^1(\Omega)} \|v\|_{\mathbb{H}^1(\Omega)}} > 0. \tag{26}$$

Proof:
Assume that the inf-sup constant above vanishes for some $h > 0$. This implies in particular that there exists $u \in \mathbb{V}_h(\Omega) \setminus \{0\}$ such that $a(u,v) - it_h(u|_\Sigma, v|_\Sigma) = 0 \ \forall v \in \mathbb{V}_h(\Omega)$. Since $\Im m\{\kappa^2\} \geq 0$ according to Assumption 1.1-*(i)*, we have $0 = \int_\Omega \Im\mathrm{m}\{\kappa(\boldsymbol{x})^2\}|u|^2 \,\mathrm{d}\boldsymbol{x} + \int_{\partial\Omega} \Re\mathrm{e}\{\kappa\}|u|^2 \,\mathrm{d}\sigma + t_h(u|_\Sigma, u|_\Sigma)$ hence $t_h(u|_\Sigma, u|_\Sigma) = 0 \Rightarrow u|_\Sigma = 0$. From this and Lemma 6.1, we conclude that $u \in \mathrm{V}_h(\Omega)$, and it satisfies $a(u,v) = a(u,v) - it_h(u|_\Sigma, v|_\Sigma) = 0$ for all $v \in \mathrm{V}_h(\Omega)$. This is not possible due to Assumption 1.2. □

Whether or not the inf-sup stability pointed in the previous lemma holds uniformly in h is a legitimate question. Because our assumptions on $t_h(\cdot,\cdot)$ are rather loose though, it is difficult to discuss this at present stage. This uniform stability shall be examined when we discuss concrete choices of $t_h(\cdot,\cdot)$ later on.

8 Reduction to a problem on the skeleton

Well-posedness of sub-problems allows to introduce local scattering operators that eliminate volume unknowns, expressing $\mathfrak{p}$ in terms of u.

Lemma 8.1 (Scattering operator)
Under Assumptions 1.1, 1.2 and 5.1, let $\mathrm{S}_h : \mathbb{V}_h(\Sigma) \to \mathbb{V}_h(\Sigma)$ *refer to the continuous operator defined by* $\mathrm{S}_h(\mathfrak{p}) = \mathfrak{p} + 2iw|_\Sigma$ *where* w *is the unique element of* $\mathbb{V}_h(\Omega)$ *satisfying* $a(w,v) - it_h(w|_\Sigma, v|_\Sigma) = t_h(\mathfrak{p}, v|_\Sigma)\ \forall v \in \mathbb{V}_h(\Omega)$. *Then we have* $\|\mathrm{S}_h(\mathfrak{p})\|_{t_h} \leq \|\mathfrak{p}\|_{t_h}\ \forall \mathfrak{p} \in \mathbb{V}_h(\Sigma)$.

Proof:
From the definition of $w \in \mathbb{V}_h(\Omega)$ we deduce that $a(w,w) - it_h(w|_\Sigma, w|_\Sigma) = t_h(\mathfrak{p}, w|_\Sigma)$. The properties of $a(\cdot,\cdot)$ then guarantee $\Im m\{a(w,w)\} \leq 0$ which leads to the inequality $-\Re e\{it_h(\mathfrak{p}, w|_\Sigma)\} = \Im m\{t_h(\mathfrak{p}, w|_\Sigma)\} \leq -\|w|_\Sigma\|^2_{t_h}$. Next, developing the expression of the norm and using the previous inequality, we obtain $\|\mathfrak{p} + 2iw|_\Sigma\|^2_{t_h} = \|\mathfrak{p}\|^2_{t_h} - 4\Re e\{it_h(\mathfrak{p}, w|_\Sigma)\} + 4\|w|_\Sigma\|^2_{t_h} \leq \|\mathfrak{p}\|^2_{t_h}$. □

We call S_h the scattering operator because it implements an ingoing-to-outgoing map i.e. it takes a tuple of ingoing traces $\mathfrak{p}$ as input, solves the associated (discrete) Helmholtz problem with ingoing Robin traces in each subdomain, and returns $\mathfrak{p} + 2iw|_\Sigma$ which is the corresponding tuple of outgoing Robin traces. The contraction property that we have just established relates to energy conservation in each subdomain. The scattering operator can be used to eliminate volume unknowns in Formulation (25) and re-write it as an equation posed on the skeleton Σ only.

Proposition 8.2
Under Assumption 1.1, 1.2 and 5.1, let $u_\star \in \mathbb{V}_h(\Omega)$ *satisfy* $a(u_\star, v) - it_h(u_\star|_\Sigma, v|_\Sigma) = \ell(v)\ \forall v \in \mathbb{V}_h(\Omega)$ *and set* $\mathfrak{f} := -2i\Pi(u_\star|_\Sigma)$. *If the pair* $(u, \mathfrak{p}) \in \mathbb{V}_h(\Omega) \times \mathbb{V}_h(\Sigma)$ *solves* (25) *then we have*

$$\begin{aligned} &\mathfrak{p} \in \mathbb{V}_h(\Sigma) \text{ such that} \\ &(\mathrm{Id} + \Pi\mathrm{S}_h)\mathfrak{p} = \mathfrak{f}. \end{aligned} \tag{27}$$

Reciprocally if $\mathfrak{p} \in \mathbb{V}_h(\Sigma)$ *solves* (27), *and if* $u \in \mathbb{V}_h(\Omega)$ *satisfies* $a(u,v) - it_h(u|_\Sigma, v|_\Sigma) = t_h(\mathfrak{p}, v|_\Sigma) + \ell(v)\ \forall v \in \mathbb{V}_h(\Omega)$, *then the pair* $(u, \mathfrak{p}) \in \mathbb{V}_h(\Omega) \times \mathbb{V}_h(\Sigma)$ *solves* (25).

In this proposition, the unique solvability of problems of the form "find $w \in \mathbb{V}_h(\Omega)$ such that $a(w,v) - it_h(w|_\Sigma, v|_\Sigma) = \text{rhs}$" is guaranteed by Lemma 7.4. Equation (27) is a reformulation of (25) as a problem posed on the skeleton Σ. It is well posed, no matter the right hand side.

Proposition 8.3 (Well posedness of the skeleton formulation)
Under Assumptions 1.1, 1.2 and 5.1, the operator $\mathrm{Id} + \Pi\mathrm{S}_h : \mathbb{V}_h(\Sigma) \to \mathbb{V}_h(\Sigma)$ *is bijective.*

Proof:
Since $\dim \mathbb{V}_h(\Sigma) < +\infty$ we only need to prove that $\ker(\mathrm{Id} + \Pi\mathrm{S}_h) = \{0\}$. Assume $\mathfrak{p} \in \mathbb{V}_h(\Sigma)$ satisfies $(\mathrm{Id} + \Pi\mathrm{S}_h)\mathfrak{p} = 0$. According to Lemma 7.4, there exists a unique $u \in \mathbb{V}_h(\Omega)$ solving $a(u,v) - it_h(u|_\Sigma, v|_\Sigma) = t_h(\mathfrak{p}, v|_\Sigma)\ \forall v \in \mathbb{V}_h(\Sigma)$. Then the pair $(u, \mathfrak{p}) \in \mathbb{V}_h(\Omega) \times \mathbb{V}_h(\Sigma)$ solves (25) with $\ell \equiv 0$. Since we have established equivalence between (25) and (4), see in particular Proposition 7.2, we conclude that u actually belongs to $\mathrm{V}_h(\Omega)$ and solves (4) with right-hand side $\ell \equiv 0$. Hence $u = 0$ according to Assumption 1.2, and thus $\mathfrak{p} = 0$ since $t_h(\mathfrak{p}, v|_\Sigma) = 0\ \forall v \in \mathbb{V}_h(\Omega)$. □

The operator $\mathrm{Id} + \mathit{\Pi}\mathrm{S}_h$ admits a special structure "*identity+contraction*". This allows to prove its strong coercivity.

Corollary 8.4
Under Assumptions 1.1, 1.2 and 5.1 we have

$$\begin{aligned} &\Re e\{t_h(\mathfrak{p}, (\mathrm{Id} + \mathit{\Pi}\mathrm{S}_h)\mathfrak{p})\} \geq \frac{\gamma_h^2}{2}\|\mathfrak{p}\|_{t_h}^2 \quad \forall \mathfrak{p} \in \mathbb{V}_h(\Sigma) \\ &\textit{where} \quad \gamma_h := \inf_{\mathfrak{w}\in\mathbb{V}_h(\Sigma)\setminus\{0\}} \|(\mathrm{Id} + \mathit{\Pi}\mathrm{S}_h)\mathfrak{w}\|_{t_h}/\|\mathfrak{w}\|_{t_h} > 0. \end{aligned} \tag{28}$$

Proof:
Due to the contractivity properties given by the Lemmas 6.2 and 8.1, we have

$$\begin{aligned} \|\mathfrak{p}\|_{t_h}^2 \geq \|\mathit{\Pi}\mathrm{S}_h(\mathfrak{p})\|_{t_h}^2 &= \|((\mathrm{Id} + \mathit{\Pi}\mathrm{S}_h) - \mathrm{Id})\mathfrak{p}\|_{t_h}^2 \\ &= \|(\mathrm{Id} + \mathit{\Pi}\mathrm{S}_h)\mathfrak{p}\|_{t_h}^2 + \|\mathfrak{p}\|_{t_h}^2 - 2\Re e\{t_h(\mathfrak{p}, (\mathrm{Id} + \mathit{\Pi}\mathrm{S}_h)\mathfrak{p})\}. \end{aligned}$$

The result then comes when eliminating $\|\mathfrak{p}\|_{t_h}^2$ from both sides of the inequality and using the definition of γ_h. □

9 Convergent iterative algorithm

Usual iterative methods can be used to compute the solution to Problem (25) or one of the equivalent forms we have obtained for it. Here we examine the convergence of a Richardson's strategy: considering[1] a fixed relaxation parameter $r \in (0, 1)$, and starting from given initial data $u^{(0)}, \mathfrak{p}^{(0)}$, we consider the algorithm

$$\begin{aligned} &(u^{(n)}, \mathfrak{p}^{(n)}) \in \mathbb{V}_h(\Omega) \times \mathbb{V}_h(\Sigma) \ \text{ and} \\ &\textit{(i)} \quad a(u^{(n)}, v) - it_h(u^{(n)}|_\Sigma, v|_\Sigma) = t_h(\mathfrak{p}^{(n)}, v|_\Sigma) + \ell(v) \quad \forall v \in \mathbb{V}_h(\Omega), \\ &\textit{(ii)} \quad \mathfrak{p}^{(n)} = (1 - r)\mathfrak{p}^{(n-1)} - r\mathit{\Pi}(\mathfrak{p}^{(n-1)} + 2iu^{(n-1)}|_\Sigma). \end{aligned} \tag{29}$$

Each step of this algorithm involves two sub-steps. The multi-trace $\mathfrak{p}^{(n)}$ should be computed first through *(ii)* which performs the exchange of information between subdomains, then $u^{(n)}$ should be computed (possibly in parallel) through *(i)*.

Remark 9.1 *Here it appears clearly why choosing diagonal impedance is interesting (cf Definition 5.6). Indeed in this case, the sesquilinear form appearing in (i) of* (29) *is itself diagonal* $a(u, v) - it_h(u|_\Sigma, v|_\Sigma) = \sum_{j=1}^{\mathrm{J}} a_{\Omega_j^h}(u, v) - it_h^j(u|_{\Gamma_j^h}, v|_{\Gamma_j^h})$. *In this situation, solving (i) reduces to computing* $u^{(n)} = (u_1^{(n)}, \ldots, u_{\mathrm{J}}^{(n)}) \in \mathbb{V}_h(\Omega)$ *where*

$$\begin{aligned} &u_j^{(n)} \in \mathrm{V}_h(\Omega_j^h) \quad \textit{and} \\ &a_{\Omega_j^h}(u_j^{(n)}, v) - it_h^j(u_j^{(n)}|_{\Gamma_j^h}, v|_{\Gamma_j^h}) = t_h^j(p_j^{(n)}, v|_{\Gamma_j^h}) + \ell_{\Omega_j^h}(v) \quad \forall v \in \mathrm{V}_h(\Omega_j^h) \end{aligned} \tag{30}$$

[1] The choice of the relaxation parameter r follows heuristic considerations. If it is chosen to fit explicit calculus for the model geometric configuration of two domains and one spherical/circular interface, the value $r = 1/\sqrt{2}$ appears to be the optimal choice, see [11].

where $\mathfrak{p}^{(n)} = (p_1^{(n)}, \dots, p_{\mathrm{J}}^{(n)})$. *Thanks to the diagonal nature of* $t_h(\cdot,\cdot)$, *such a problem must be solved for each* $j = 1 \dots \mathrm{J}$ *independently. When the impedance is diagonal, solving such problems as (i) of* (29) *is then parallel.*

This condition on the diagonal nature of the impedance is not required for the present analysis. Yet most of the impedances $t_h(\cdot,\cdot)$ *considered in practice agree with the diagonal form of Definition 5.6 and this has important practical advantages since it is more favorable to distributed-memory parallel implementations where a possible bottleneck lies in the cost of communication between processors. However, certain domain decomposition strategies consider the case where the impedance operator is not subdomain-wise block diagonal see for example [18, §3.1]. Without assuming that* $t_h(\cdot,\cdot)$ *is block diagonal though, Algorithm* (29) *raises serious computational difficulties.*

The next result shows that the iterative scheme (29) converges toward the solution of our initial boundary value problem (4) with geometric convergence.

Theorem 9.2 (Geometric convergence of Richardson algorithm)
Under Assumptions 1.1, 1.2 and 5.1, let $\mathfrak{p}^{(\infty)} \in \mathrm{V}_h(\Omega)$ *refer to the unique solution to* (27), *consider a relaxation parameter* $r \in (0,1)$ *and define* γ_h *as in* (28). *Then the iterates* $\mathfrak{p}^{(n)}$ *computed by means of* (29) *satisfy the estimate*

$$\frac{\|\mathfrak{p}^{(n)} - \mathfrak{p}^{(\infty)}\|_{t_h}}{\|\mathfrak{p}^{(0)} - \mathfrak{p}^{(\infty)}\|_{t_h}} \leq (1 - r(1-r)\gamma_h^2)^{n/2}. \tag{31}$$

Proof:
The $\mathfrak{p}^{(n)}$ defined through (29) satisfy the recurrence $\mathfrak{p}^{(n)} = (1-r)\mathfrak{p}^{(n-1)} - r\Pi\mathrm{S}_h(\mathfrak{p}^{(n-1)}) + r\mathfrak{f}$ with $\mathfrak{f} \in \mathbb{V}_h(\Sigma)$ defined as in (27). We conclude that the sequence $\epsilon_n := \mathfrak{p}^{(n)} - \mathfrak{p}^{(\infty)}$ satisfies $\epsilon_n = (1-r)\epsilon_{n-1} - r\Pi\mathrm{S}_h(\epsilon_{n-1})$. According to Lemma 6.2 and Lemma 8.1, we have $\|\Pi\mathrm{S}_h(\epsilon_{n-1})\|_{t_h} \leq \|\epsilon_{n-1}\|_{t_h}$. From this we deduce

$$\begin{aligned}
\|\epsilon_n\|_{t_h}^2 &= \|(1-r)\epsilon_{n-1} - r\Pi\mathrm{S}_h(\epsilon_{n-1})\|_{t_h}^2 \\
&= (1-r)\|\epsilon_{n-1}\|_{t_h}^2 + r\|\Pi\mathrm{S}_h(\epsilon_{n-1})\|_{t_h}^2 \\
&\qquad - r(1-r)\|(\mathrm{Id} + \Pi\mathrm{S}_h)\epsilon_{n-1}\|_{t_h}^2 \\
&\leq (1 - r(1-r)\gamma_h^2)\|\epsilon_{n-1}\|_{t_h}^2.
\end{aligned}$$

□

Note that the constant $(1-r(1-r)\gamma_h^2)$ is positive, since $\gamma_h \leq 2$ from the Lemmas 6.2 and 8.1. Proposition 8.3 guarantees that $\gamma_h > 0$ in the previous result. This a priori does not discard the possibility that $\lim_{h\to 0}\gamma_h = 0$ and $\lim_{h\to 0}(1-\gamma_h^2 r(1-r)) = 1$ which would correspond to a deterioration in the convergence of (29). On the other hand, if γ_h can be proved to remain bounded away from 0, this will correspond to h-uniform geometric convergence. Through the solution to local sub-problems, the previous theorem also yields a convergence estimate for $u^{(n)}$.

Corollary 9.3
Under Assumptions 1.1,1.2 and 5.1, let $(u^{(\infty)}, \mathfrak{p}^{(\infty)})$ *refer to the unique solution to* (25), *and suppose that the sequence* $(u^{(n)}, \mathfrak{p}^{(n)})$ *has been defined through* (29).

Define γ_h as in (28)*, let β_h refer to the inf-sup constant of Lemma 7.4, and define λ_h^+ as in* (15)*. Then we have the estimate*

$$\frac{\|u^{(n)} - u^{(\infty)}\|_{\mathbb{H}^1(\Omega)}}{\|\mathfrak{p}^{(0)} - \mathfrak{p}^{(\infty)}\|_{t_h}} \leq \frac{\lambda_h^+}{\beta_h}(1 - r(1-r)\gamma_h^2)^{n/2}.$$

Proof:

Set $e_n := u^{(n)} - u^{(\infty)}$ and $\epsilon_n := \mathfrak{p}^{(n)} - \mathfrak{p}^{(\infty)}$. Combining (29) with (25) we obtain that $a(e_n, v) - it_h(e_n|_\Sigma, v|_\Sigma) = t_h(\epsilon_n, v|_\Sigma)$ for all $v \in \mathbb{V}_h(\Omega)$. We have $\|v|_\Sigma\|_{\rho_h} \leq \|v\|_{\mathbb{H}^1(\Omega)}$ according to (9)-(10). Thus, using the inf-sup constant from Lemma 7.4, and the continuity modulus of t_h, we obtain $\beta_h\|e_n\|_{\mathbb{H}^1(\Omega)} \leq \lambda_h^+\|\epsilon_n\|_{t_h}$. There only remains to apply Theorem 9.2. □

10 Discrete stability

The inf-sup constant (noted γ_h) of the operator $\mathrm{Id} + \Pi\mathrm{S}_h$, plays a crucial role in the bound for the convergence rate provided by Theorem 9.2. In the present section we analyze in more detail this quantity.

Remark 10.1 *Besides γ_h defined by* (28)*, the forthcoming stability and convergence analysis will repeatedly refer to the following constants:*

- *α_h defined through Assumption 1.2,*
- *$\|a\|$ defined by* (22)*,*
- *β_h defined by* (26)*,*
- *$\lambda_h^\pm$ defined by* (15)*.*

These constants a priori depend, not only on the mesh width parameter h, but also on the material characteristics, including the wave number κ, and the geometry of the computational domain.

We first need to introduce $\mathbb{V}_h(\Sigma)^2 := \mathbb{V}_h(\Sigma) \times \mathbb{V}_h(\Sigma)$ equipped with the cartesian product norm defined by

$$\|(\mathfrak{p}, \mathfrak{q})\|_{t_h^2}^2 := \|\mathfrak{p}\|_{t_h}^2 + \|\mathfrak{q}\|_{t_h}^2.$$

We shall proceed by imitating the analytical approach presented in [8], which leads to introducing two subspaces

$$\begin{aligned}
&\mathscr{V}_h(\Sigma) := \mathrm{V}_h(\Sigma) \times \mathrm{V}_h(\Sigma)^\perp,\\
&\mathscr{C}_h(\Sigma) := \{\ (\mathfrak{u}_\mathrm{D}, \mathfrak{u}_\mathrm{N}) \in \mathbb{V}_h(\Sigma)^2 :\ \exists u \in \mathbb{V}_h(\Omega) \text{ such that } u|_\Sigma = \mathfrak{u}_\mathrm{D}\\
&\qquad\qquad \text{and } a(u, v) = t_h(\mathfrak{u}_\mathrm{N}, v|_\Sigma)\ \forall v \in \mathbb{V}_h(\Omega)\ \}.
\end{aligned}$$

These are discrete counterparts of the single-trace and Cauchy data spaces considered in Section 4 and 6 of [8]. These are two complementary subspaces of the (discrete) multi-trace space.

Proposition 10.2
Under Assumptions 1.1, 1.2 and 5.1, we have $\mathbb{V}_h(\Sigma) \times \mathbb{V}_h(\Sigma) = \mathscr{V}_h(\Sigma) \oplus \mathscr{C}_h(\Sigma)$. *Moreover, if* $\mathrm{P}_h : \mathbb{V}_h(\Sigma) \times \mathbb{V}_h(\Sigma) \to \mathscr{C}_h(\Sigma)$ *is the projection onto* $\mathscr{C}_h(\Sigma)$ *with* $\ker(\mathrm{P}_h) = \mathscr{V}_h(\Sigma)$, *then*

$$\sup_{(\mathfrak{p},\mathfrak{q})\in\mathbb{V}_h(\Omega)^2\setminus\{0\}} \frac{\|\mathrm{P}_h(\mathfrak{p},\mathfrak{q})\|_{t_h^2}}{\|(\mathfrak{p},\mathfrak{q})\|_{t_h^2}} \leq \frac{(\lambda_h^+)^2 + (2\|a\|/\lambda_h^-)^2}{\alpha_h}. \tag{32}$$

Proof:
Assume first that $(\mathfrak{p},\mathfrak{q}) \in \mathscr{V}_h(\Sigma) \cap \mathscr{C}_h(\Sigma)$. By definition of $\mathscr{C}_h(\Sigma)$, there exists $u \in \mathbb{V}_h(\Omega)$ satisfying $u|_\Sigma = \mathfrak{p}$ and $a(u,v) = t_h(\mathfrak{q}, v|_\Sigma)\ \forall v \in \mathbb{V}_h(\Omega)$. From $\mathfrak{p} \in \mathrm{V}_h(\Sigma)$ and Lemma 6.1, we conclude that $u \in \mathrm{V}_h(\Omega)$, and since $\mathfrak{q} \in \mathrm{V}_h(\Sigma)^\perp$, we have $a(u,v) = 0 \forall v \in \mathrm{V}_h(\Omega)$. Hence $u = 0$ according to Assumption 1.2, and thus $\mathfrak{p} = \mathfrak{q} = 0$. This proves that $\mathscr{V}_h(\Sigma) \cap \mathscr{C}_h(\Sigma) = \{0\}$.

Next we prove that $\mathbb{V}_h(\Sigma)\times\mathbb{V}_h(\Sigma) = \mathscr{V}_h(\Sigma)+\mathscr{C}_h(\Sigma)$. Pick $(\mathfrak{p},\mathfrak{q}) \in \mathbb{V}_h(\Sigma)\times\mathbb{V}_h(\Sigma)$ arbitrarily, and define ψ as the unique solution to $\psi \in \mathrm{V}_h(\Omega)$ and $a(\psi+\rho_h(\mathfrak{p}), v) = t_h(\mathfrak{q}, v|_\Sigma)\ \forall v \in \mathrm{V}_h(\Omega)$ according to Assumption 1.2. This function is bounded by

$$\|\psi\|_{\mathrm{H}^1(\Omega)} \leq \Big(\frac{\|a\|}{\alpha_h\lambda_h^-}\Big)\|\mathfrak{p}\|_{t_h} + \frac{\lambda_h^+}{\alpha_h}\|\mathfrak{q}\|_{t_h}. \tag{33}$$

Next rewriting $u := \psi + \rho_h(\mathfrak{p})$, we set $\mathfrak{u}_\mathrm{D} := u|_\Sigma$. In addition, we have $a(u,w) = 0$ for all $w \in \mathrm{V}_h(\Omega)$ satisfying $w|_\Sigma = 0$ so, according to Lemma 5.7, we can define $\mathfrak{u}_\mathrm{N}$ as the unique element of $\mathbb{V}_h(\Sigma)$ satisfying $t_h(\mathfrak{u}_\mathrm{N}, v|_\Sigma) = a(u,v)\ \forall v \in \mathbb{V}_h(\Omega)$ and actually $t_h(\mathfrak{u}_\mathrm{N}, \mathfrak{w}) = a(u, \rho_h(\mathfrak{w}))\ \forall \mathfrak{w} \in \mathbb{V}_h(\Sigma)$. We deduce the estimates

$$\begin{aligned}
&\|u\|_{\mathbb{H}^1(\Omega)} \leq \|\psi\|_{\mathrm{H}^1(\Omega)} + \|\mathfrak{p}\|_{t_h}/\lambda_h^-,\\
&\|\mathfrak{u}_\mathrm{D}\|_{t_h} \leq \lambda_h^+\|u\|_{\mathbb{H}^1(\Omega)},\\
&\|\mathfrak{u}_\mathrm{N}\|_{t_h} \leq (\|a\|/\lambda_h^-)\|u\|_{\mathbb{H}^1(\Omega)}.
\end{aligned} \tag{34}$$

Now observe that $(\mathfrak{u}_\mathrm{D}, \mathfrak{u}_\mathrm{N}) \in \mathscr{C}_h(\Sigma)$ by construction. Besides we have $\mathfrak{p} - \mathfrak{u}_\mathrm{D} = \rho_h(\mathfrak{p})|_\Sigma - \mathfrak{u}_\mathrm{D} = -\psi|_\Sigma \in \mathrm{V}_h(\Sigma)$ since $\psi \in \mathrm{V}_h(\Omega)$. Finally we have $t_h(\mathfrak{q}-\mathfrak{u}_\mathrm{N}, v|_\Sigma) = 0$ for all $v \in \mathrm{V}_h(\Omega)$ so that $\mathfrak{q} - \mathfrak{u}_\mathrm{N} \in \mathrm{V}_h(\Sigma)^\perp$. We conclude that $(\mathfrak{p},\mathfrak{q}) - (\mathfrak{u}_\mathrm{D}, \mathfrak{u}_\mathrm{N}) \in \mathscr{V}_h(\Sigma)$ and thus $(\mathfrak{u}_\mathrm{D}, \mathfrak{u}_\mathrm{N}) = \mathrm{P}_h(\mathfrak{p},\mathfrak{q})$. Finally Estimate (32) is obtained by combining (33) with (34) and observing that $\|a\|/\alpha_h \geq 1$ systematically. □

Next we point that $\mathscr{C}_h(\Sigma)$ is closely related to the graph of the scattering operator S_h, as confirmed by the next lemma.

Lemma 10.3
Under Assumptions 1.1, 1.2 and 5.1, we have
$\mathscr{C}_h(\Sigma) = \{(\mathfrak{u}_\mathrm{D}, \mathfrak{u}_\mathrm{N}) \in \mathbb{V}_h(\Sigma) \times \mathbb{V}_h(\Sigma) :\ \mathfrak{u}_\mathrm{N} + i\mathfrak{u}_\mathrm{D} = \mathrm{S}_h(\mathfrak{u}_\mathrm{N} - i\mathfrak{u}_\mathrm{D})\}$.

Proof:
Take any $(\mathfrak{u}_\mathrm{D}, \mathfrak{u}_\mathrm{N}) \in \mathscr{C}_h(\Sigma)$. By definition there exists $u \in \mathbb{V}_h(\Omega)$ such that $u|_\Sigma = \mathfrak{u}_\mathrm{D}$ and $a(u,v) = t_h(\mathfrak{u}_\mathrm{N}, v|_\Sigma)$ for all $v \in \mathbb{V}_h(\Omega)$. This implies $a(u,v) - it_h(u|_\Sigma, v|_\Sigma) = t_h(\mathfrak{u}_\mathrm{N} - i\mathfrak{u}_\mathrm{D}, v|_\Sigma)\ \forall v \in \mathbb{V}_h(\Omega)$. Hence we have $\mathrm{S}_h(\mathfrak{u}_\mathrm{N} - i\mathfrak{u}_\mathrm{D}) = \mathfrak{u}_\mathrm{N} - i\mathfrak{u}_\mathrm{D} + 2iu|_\Sigma = \mathfrak{u}_\mathrm{N} + i\mathfrak{u}_\mathrm{D}$ according to the definition of the scattering operator given by Lemma 8.1.

Reciprocally, assume that $(\mathfrak{u}_{\mathrm{D}}, \mathfrak{u}_{\mathrm{N}}) \in \mathbb{V}_h(\Sigma)$ satisfies $\mathfrak{u}_{\mathrm{N}} + i\mathfrak{u}_{\mathrm{D}} = \mathrm{S}_h(\mathfrak{u}_{\mathrm{N}} - i\mathfrak{u}_{\mathrm{D}})$. Defining u as the unique element of $\mathbb{V}_h(\Omega)$ solving $a(u,v) - it_h(u|_\Sigma, v|_\Sigma) = t_h(\mathfrak{u}_{\mathrm{N}} - i\mathfrak{u}_{\mathrm{D}}, v|_\Sigma)\ \forall v \in \mathbb{V}_h(\Sigma)$, we have $\mathfrak{u}_{\mathrm{N}} + i\mathfrak{u}_{\mathrm{D}} = \mathfrak{u}_{\mathrm{N}} - i\mathfrak{u}_{\mathrm{D}} + 2iu|_\Sigma \Rightarrow \mathfrak{u}_{\mathrm{D}} = u|_\Sigma$. From this we also deduce $a(u,v) = t_h(\mathfrak{u}_{\mathrm{N}}, v|_\Sigma)$ for all $v \in \mathbb{V}_h(\Omega)$. Hence $(\mathfrak{u}_{\mathrm{D}}, \mathfrak{u}_{\mathrm{N}}) \in \mathscr{C}_h(\Sigma)$.

□

The projection we have defined in Proposition 10.2 leads to an explicit expression of the inverse operator $(\mathrm{Id} + \mathit{\Pi}\mathrm{S}_h)^{-1}$, which we can use to bound the corresponding inf-sup constant.

Proposition 10.4
Under Assumptions 1.1, 1.2 and 5.1, we have

$$\gamma_h := \inf_{\mathfrak{w} \in \mathbb{V}_h(\Sigma)\setminus\{0\}} \frac{\|(\mathrm{Id} + \mathit{\Pi}\mathrm{S}_h)\mathfrak{w}\|_{t_h}}{\|\mathfrak{w}\|_{t_h}} \geq \frac{\sqrt{2}\,\alpha_h}{(\lambda_h^+)^2 + (2\|a\|/\lambda_h^-)^2}.$$

Proof:

Pick an arbitrary $\mathfrak{f} \in \mathbb{V}_h(\Sigma)$ and set $\mathfrak{p}_{\mathrm{D}} = i(\mathrm{Id} - \mathit{\Pi})\mathfrak{f}/4$, $\mathfrak{p}_{\mathrm{N}} = (\mathrm{Id} + \mathit{\Pi})\mathfrak{f}/4$. Next, considering the projection introduced in Proposition 10.2, define $(\mathfrak{u}_{\mathrm{D}}, \mathfrak{u}_{\mathrm{N}}) := \mathrm{P}_h(\mathfrak{p}_{\mathrm{D}}, \mathfrak{p}_{\mathrm{N}}) \in \mathscr{C}_h(\Sigma)$. By construction we have $\mathfrak{u}_{\mathrm{D}} - \mathfrak{p}_{\mathrm{D}} \in \mathrm{V}_h(\Sigma)$ and $\mathfrak{u}_{\mathrm{N}} - \mathfrak{p}_{\mathrm{N}} \in \mathrm{V}_h(\Sigma)^\perp$. Applying Lemma 6.2, we obtain

$$\begin{aligned}
&-(\mathfrak{u}_{\mathrm{N}} - \mathfrak{p}_{\mathrm{N}}) + i(\mathfrak{u}_{\mathrm{D}} - \mathfrak{p}_{\mathrm{D}}) = \mathit{\Pi}\big((\mathfrak{u}_{\mathrm{N}} - \mathfrak{p}_{\mathrm{N}}) + i(\mathfrak{u}_{\mathrm{D}} - \mathfrak{p}_{\mathrm{D}})\big)\\
\iff\ &\mathfrak{u}_{\mathrm{N}} - i\mathfrak{u}_{\mathrm{D}} + \mathit{\Pi}(\mathfrak{u}_{\mathrm{N}} + i\mathfrak{u}_{\mathrm{D}}) = (\mathrm{Id} + \mathit{\Pi})\mathfrak{p}_{\mathrm{N}} - i(\mathrm{Id} - \mathit{\Pi})\mathfrak{p}_{\mathrm{D}}\\
&\qquad = [(\mathrm{Id} + \mathit{\Pi})/2]^2\mathfrak{f} + [(\mathrm{Id} - \mathit{\Pi})/2]^2\mathfrak{f}\\
&\qquad = (\mathrm{Id} + \mathit{\Pi})\mathfrak{f}/2 + (\mathrm{Id} - \mathit{\Pi})\mathfrak{f}/2 = \mathfrak{f}.
\end{aligned}$$

Applying Lemma 10.3, we conclude that $(\mathrm{Id} + \mathit{\Pi}\mathrm{S}_h)(\mathfrak{u}_{\mathrm{N}} - i\mathfrak{u}_{\mathrm{D}}) = \mathfrak{f}$ which rewrites $\mathfrak{u}_{\mathrm{N}} - i\mathfrak{u}_{\mathrm{D}} = (\mathrm{Id} + \mathit{\Pi}\mathrm{S}_h)^{-1}\mathfrak{f}$.

Now, observe that, due to the orthogonality of the projectors $(\mathrm{Id} \pm \mathit{\Pi})/2$ for the scalar product induced by t_h (Lemma 6.2), we have $\|(\mathfrak{p}_{\mathrm{D}}, \mathfrak{p}_{\mathrm{N}})\|_{t_h^2}^2 = \|\mathfrak{p}_{\mathrm{D}}\|_{t_h}^2 + \|\mathfrak{p}_{\mathrm{N}}\|_{t_h}^2 = \|\mathfrak{f}\|_{t_h}^2/4$. Finally, using Proposition 10.2, we obtain the estimate

$$\begin{aligned}
\|(\mathrm{Id} + \mathit{\Pi}\mathrm{S}_h)^{-1}\mathfrak{f}\|_{t_h} &= \|\mathfrak{u}_{\mathrm{N}} - i\mathfrak{u}_{\mathrm{D}}\|_{t_h}\\
&\leq \sqrt{2}\|(\mathfrak{u}_{\mathrm{D}}, \mathfrak{u}_{\mathrm{N}})\|_{t_h^2} = \sqrt{2}\|\mathrm{P}_h(\mathfrak{p}_{\mathrm{D}}, \mathfrak{p}_{\mathrm{N}})\|_{t_h^2}\\
&\leq \frac{(\lambda_h^+)^2 + (2\|a\|/\lambda_h^-)^2}{\sqrt{2}\alpha_h}\|\mathfrak{f}\|_{t_h}.
\end{aligned}$$

□

Remark 10.5 *Proposition 10.4 is instructive from the perspective of wave-number dependency. Indeed, there is no hidden constant in the estimate provided for γ_h. Since this result holds under Assumptions 1.1, 1.2 and 5.1 only, Proposition 10.4 remains valid when the mesh width h and the wave number κ both vary simultaneously. In other words Proposition 10.4 seems useful for investigating Optimized Schwarz Methods in the high frequency regime.*

In a situation where both h and κ vary, a deterioration of the lower bound for γ_h can only come from $\alpha_h, \|a\|$ or $\lambda_h^\pm$. The (κ, h)-behavior of $\lambda_h^\pm$ of course totally depends on the choice of impedance $t_h(\cdot,\cdot)$ and nothing can be inferred without being more specific on this choice. Let us point that the choice of impedance

corresponding to $t_h(\mathfrak{p},\mathfrak{p}) = \|\mathfrak{p}\|^2_{\rho_h}$ *from Example 5.5 leads to* $\lambda_h^{\pm} = 1$ *which is clearly* (κ,h)*-uniform. The bound* $\|a\|$ *can be considered harmless regarding* (κ,h)*-dependency (see Remark 7.1). Then only the* (κ,h)*-behavior of* α_h *remains to be analyzed. Understanding the behavior of this discrete inf-sup constant for large wave numbers is a non-trivial issue, beyond the scope of the present article, and this is the subject of active research at present, see [28, 35].*

Combining Proposition 10.4 with Lemma 8.4 or Theorem 9.2 obviously yields an estimate for the convergence rate of linear iterative solvers. In particular, when the impedance is chosen as equivalent to the scalar product associated to $\|\cdot\|_{\rho_h}$, convergence is then uniform with respect to the discretization parameter. This motivates to introduce the following condition. We will systematically state explicitly when this condition is necessary (but it is not assumed to hold in general).

Condition 10.6 (h-uniformly stable impedance)
The impedance operator is such that
$\lambda_\star^- := \liminf_{h\to 0}\lambda_h^- > 0$ *and* $\lambda_\star^+ := \limsup_{h\to 0}\lambda_h^+ < +\infty$.

Corollary 10.7
Under Assumptions 1.1, 1.2 and 5.1 let $\mathfrak{p}^{(\infty)} \in \mathrm{V}_h(\Omega)$ *refer to the unique solution to* (27)*, consider the relaxation parameter* $r \in (0,1)$*. Assume in addition that material characteristics (in particular* κ*) are fixed and that Condition 10.6 holds. Then* $0 < \liminf_{h\to 0}\gamma_h$ *and for any* $0 < \gamma_\star < \liminf_{h\to 0}\gamma_h$ *there exists* $h_\star > 0$ *such that the iterates* $\mathfrak{p}^{(n)}$ *computed by means of* (29) *satisfy the estimate*

$$\frac{\|\mathfrak{p}^{(n)} - \mathfrak{p}^{(\infty)}\|_{t_h}}{\|\mathfrak{p}^{(0)} - \mathfrak{p}^{(\infty)}\|_{t_h}} \leq (1 - r(1-r)\gamma_\star^2)^{n/2} \quad \forall h \in (0,h_\star), \forall n \geq 0. \tag{35}$$

11 Fixed geometric partitions

In the present section, to obtain explicit results, we assume that Condition 2.1 holds, which corresponds to the situation of Figure 1a. This implies in particular that the number J of subdomains remains bounded. Besides, we shall also rely on a further condition regarding the impedance operator t_h.

Condition 11.1
There exists a continuous positive definite sesquilinear form $t(\cdot,\cdot) : \mathbb{H}^{1/2}(\Sigma) \times \mathbb{H}^{1/2}(\Sigma) \to \mathbb{C}$ *independent of h, and two constants* $c_\pm > 0$ *independent of h, such that* $c_- \leq t_h(\mathfrak{p},\mathfrak{p})/t(\mathfrak{p},\mathfrak{p}) \leq c_+$ *for all* $\mathfrak{p} \in \mathbb{V}_h(\Sigma)\setminus\{0\}$ *and all* $h > 0$.

This condition simply means that the discrete impedance operator is equivalent to a continuous counterpart that is independent of the mesh. Després impedance (Example 5.2) and integral operator based impedances (Example 5.4) fulfill this condition. Under the additional condition of h-uniform shape regularity (11), the Schur complement based impedance (Example 5.5) also fulfills Condition 11.1.

Lemma 11.2
Assume that Assumptions 1.1, 1.2 and Conditions 2.1, 11.1 are satisfied. Then the inf-sup constant β_h *defined in equation* (26) *is asymptotically h-uniformly bounded from below* $\beta_\star = \liminf_{h\to 0}\beta_h > 0$.

Proof:

We proceed by contradiction, assuming that there exist sequences $h_n \to 0$ and $u_n \in \mathbb{V}_{h_n}(\Omega)$ satisfying $\|u_n\|_{\mathbb{H}^1(\Omega)} = 1$ and

$$\lim_{n\to\infty} \sup_{v\in\mathbb{V}_{h_n}(\Omega)\setminus\{0\}} |a(u_n, v) - it_{h_n}(u_n, v)|/\|v\|_{\mathbb{H}^1(\Omega)} = 0. \tag{36}$$

Assumptions 1.1 imply that $t_{h_n}(u_n, u_n) \leq |\Im m\{a(u_n, u_n) - it_{h_n}(u_n, u_n)\}|$. Combining Condition 11.1 with (36) thus leads to $t(u_n, u_n) \leq t_{h_n}(u_n, u_n)/c_- \to 0$. Cauchy-Schwarz inequality applied with $t(\cdot,\cdot)$ then shows

$$\lim_{n\to 0} t(u_n, v) = 0 \quad \forall v \in \mathbb{H}^1(\Omega). \tag{37}$$

Next, extracting a subsequence if necessary, we may assume that u_n converges toward some $u_\infty \in \mathbb{H}^1(\Omega)$ weakly in $\mathbb{H}^1(\Omega)$ such that $0 = \lim_{n\to\infty} \|u_n - u_\infty\|_{\mathrm{L}^2(\Omega)} = \lim_{n\to\infty} \|u_n - u_\infty\|_{\mathrm{L}^2(\partial\Omega)}$. According to (37) we obtain $0 = \lim_{n\to\infty} t(u_n, u_\infty) = t(u_\infty, u_\infty)$. Since $t(\cdot,\cdot)$ is positive definite on $\mathbb{H}^{1/2}(\Sigma)$, we conclude

$$t(u_\infty, v) = 0 \quad \forall v \in \mathbb{H}^1(\Omega). \tag{38}$$

Take any $v \in \mathbb{H}^1(\Omega)$ and let $v_n \in \mathbb{V}_{h_n}(\Omega)$ refer to its best approximation in the discrete variational space i.e. $\|v - v_n\|_{\mathbb{H}^1(\Omega)} = \inf\{\|v - w\|_{\mathbb{H}^1(\Omega)},\ w \in \mathbb{V}_{h_n}(\Omega)\}$. In particular we have $\|v - v_n\|_{\mathbb{H}^1(\Omega)} \to 0$. Applying Cauchy-Schwarz inequality with $t_{h_n}(\cdot,\cdot)$ and using Condition 11.1, we obtain

$$\begin{aligned} |t_{h_n}(u_n, v_n)|^2 &\leq t_{h_n}(u_n, u_n) t_{h_n}(v_n, v_n) \\ &\leq c_+ t_{h_n}(u_n, u_n) t(v_n, v_n) \to 0. \end{aligned} \tag{39}$$

Weak convergence of (u_n) together with (36), (38) and (39) implies $a(u_n, v_n) - it_{h_n}(u_n, v_n) \to 0 = a(u_\infty, v) - it(u_\infty, v)$. Since v was chosen arbitrarily in $\mathbb{H}^1(\Omega)$ we conclude that $u_\infty = 0$, which implies $\lim_{n\to\infty} \|u_n\|_{\mathrm{L}^2(\Omega)} = 0$. We finally obtain $\|u_n\|^2_{\mathbb{H}^1(\Omega)} \leq C\Re e\{a(u_n, u_n)\} + C\Re e\{\int_\Omega \kappa^2(\boldsymbol{x})|u_n|^2 \ \mathrm{d}\boldsymbol{x}\} + \kappa_\infty^2 \|u_n\|^2_{\mathrm{L}^2(\Omega)}$ where $C = \sup_\Omega |\mu^{-1}| < +\infty$ according to Assumption 1.1. Since $\Re e\{a(u_n, u_n)\} \to 0$ according to (36) and $\|u_n\|_{\mathrm{L}^2(\Omega)} \to 0$, we deduce that $\|u_n\|_{\mathbb{H}^1(\Omega)} \to 0$ which yields a contradiction. □

From Lemma 11.2 and assuming in addition uniform boundedness of the impedance operator, we easily obtain h-uniform convergence for the Richardson algorithm (29).

Corollary 11.3 (h-uniform geometric convergence for Richardson)
Under Assumptions 1.1, 1.2 and 5.1, let $(u^{(\infty)}, \mathfrak{p}^{(\infty)})$ refer to the unique solution to (25), and suppose that the sequence $(u^{(n)}, \mathfrak{p}^{(n)})$ has been defined through (29). Assume in addition that material characteristics (in particular κ) are fixed; that Conditions 2.1, 10.6 and 11.1 are satisfied and recall the definition of $\beta_\star$ from Lemma 11.2. Then $0 < \liminf_{h\to 0} \gamma_h$ and for any $0 < \gamma_\star < \liminf_{h\to 0} \gamma_h$ there exists $h_\star > 0$ such that

$$\frac{\|u^{(n)} - u^{(\infty)}\|_{\mathbb{H}^1(\Omega)}}{\|\mathfrak{p}^{(0)} - \mathfrak{p}^{(\infty)}\|_{t_h}} \leq \frac{\lambda_\star^+}{\beta_\star}(1 - r(1-r)\gamma_\star^2)^{n/2} \quad \forall h \in (0, h_\star), \forall n \geq 0. \tag{40}$$

Now let us examine how the estimates of the previous and current sections apply for the concrete choice of impedance considered in Section 5.

Example 11.4 (Després impedance) *In the case of a fixed geometric partition (Condition 2.1) and fixed material characteristics, the Després impedance from Example 5.2 fits within the assumptions (in particular Condition 11.1) of Lemma 11.2. However, this choice of impedance violates Condition 10.6, hence the assumptions of both results that guarantee h-uniform convergence rate Corollary 10.7 and Corollary 11.3.*

It is remarkable that our analysis provides nevertheless explicit upper bounds for the convergence factor that give insights on the deterioration of the rate of convergence when using this operator. Indeed, for this choice of impedance, we have $\lambda_h^- = \mathcal{O}(\sqrt{h})$ *and* $\limsup_{h\to 0} \lambda_h^+ < +\infty$*, so that* $\gamma_h \geq ch$ *for a constant* $c > 0$ *independent of* h *according to Proposition 10.4. Hence, under the conditions of Theorem 9.2, Algorithm* (29) *with Després impedance satisfies the following convergence estimate*

$$\frac{\|\mathfrak{p}^{(n)} - \mathfrak{p}^{(\infty)}\|_{t_h}}{\|\mathfrak{p}^{(0)} - \mathfrak{p}^{(\infty)}\|_{t_h}} \leq (1 - c^2 r(1-r)h^2)^{n/2}, \tag{41}$$

and a similar estimate holds for $\|u^{(n)} - u^{(\infty)}\|_{\mathbb{H}^1(\Omega)}$*, see Corollary 9.3. Therefore, although convergence does hold with Després transmission condition, our theory suggests a deterioration in the convergence rate for* $h \to 0$*. The convergence factor upper bound* $\tau := (1 - c^2 r(1-r)h^2)^{1/2}$ *behaves asymptotically like* $1 - \mathcal{O}(h^2)$ *as* h *goes to* 0*. It shall be noticed that convergence factors with such asymptotic behavior necessarily induce a quadratic growth of the number of iterations required to obtain convergence to a fixed tolerance. If we cannot say anything on the sharpness of the upper bound estimate, this type of deterioration is somehow visible on our numerical examples (which were however not obtained under Condition 2.1), for instance in Figure 5a.*

Example 11.5 (Second order differential operator) *In the case of a fixed geometric partition (Condition 2.1) and fixed material characteristics, impedance condition of second order* (17) *from Example 5.3 violates both Conditions 10.6 and 11.1, hence the assumptions of both results that guarantee h-uniform convergence rate Corollary 10.7 and Corollary 11.3.*

Again, our analysis provides insights on the deterioration of the rate of convergence when using this operator. In this case we have $\liminf_{h\to 0} \lambda_h^- > 0$ *and* $\limsup_{h\to 0} \lambda_h^+ = \mathcal{O}(1/\sqrt{h})$ *so that, as in the previous example,* $\gamma_h \geq ch$ *for a constant* $c > 0$ *independent of* h*, and* (41) *holds. Unlike the preceding example though, we cannot prove h-uniform discrete local inf-sup stability i.e.* $\beta_\star > 0$ *as given by Lemma 11.2 hence, in contrast with* $\|\mathfrak{p}^{(n)} - \mathfrak{p}^{(\infty)}\|_{t_h}$*, one cannot claim that* $\|u^{(n)} - u^{(\infty)}\|_{\mathbb{H}^1(\Omega)}$ *satisfies an estimate similar to* (41)*. Yet, again in this case, the convergence factor upper bound behaves asymptotically like* $1 - \mathcal{O}(h^2)$ *as* h *goes to* 0*, which would induce a quadratic growth of the number of iterations required to obtain convergence to a fixed tolerance if this upper bound was describing the actual convergence rate. Once again we observe a deterioration in our numerical tests indicating that the actual convergence rate behaves similarly to the upper bound with respect to the mesh width* h*, for instance in Figure 5a.*

Example 11.6 (Integral operator based impedance) *In the case of a fixed geometric partition (Condition 2.1) and fixed material characteristics, the impedance*

based on the hypersingular integral operator (18) *from Example 5.4 satisfies both Conditions 10.6 and 11.1, in contrast with the two previous examples. Indeed, in this case, we have* $0 < \liminf_{h\to 0} \lambda_h^- $ *and* $\limsup_{h\to 0} \lambda_h^+ < +\infty$ *so that* $\gamma_\star = \liminf_{h\to 0} \gamma_h > 0$ *and we have the h-uniform convergence estimate* (35) *of Corollary 10.7. Besides, the assumptions of Lemma 11.2 are satisfied, which yields uniform discrete local inf-sup stability and the convergence estimate* (40) *holds for* $\|u^{(n)} - u^{(\infty)}\|_{\mathbb{H}^1(\Omega)}$ *according to Corollary 11.3. Our numerical results do confirm the h-uniform stability of the convergence rate.*

Example 11.7 (Schur complement based impedance) *In the case of a fixed geometric partition (Condition 2.1) and fixed material characteristics, the Schur complement based impedance* (19) *of Example 5.5 satisfies Condition 10.6 since in this case we have* $\lambda_h^\pm = 1$. *Therefore* $\gamma_\star = \liminf_{h\to 0} \gamma_h > 0$ *and the h-uniform convergence estimate* (35) *of Corollary 10.7 holds. According to Lemma 4.1, under the additional condition of h-uniform shape regularity* (11)*, this operator complies with Condition 11.1 and therefore fits the assumptions of Lemma 11.2. This allows to conclude that the convergence estimate* (40) *also holds for* $\|u^{(n)} - u^{(\infty)}\|_{\mathbb{H}^1(\Omega)}$ *according to Corollary 11.3. This is confirmed in our numerical experiments of Section 14. In fact it is remarkable that the best results are systematically associated to this choice of impedance.*

12 The case of no cross-point

The case where the subdomain partition (5) does not involve any cross-point is an important particular case, so we dedicate the present section to study this situation. The exchange operator $\mathit{\Pi}$ becomes substantially simpler in this case. By "absence of cross-point" we mean:

$$\begin{aligned} &\Gamma_j^h \cap \Gamma_k^h \cap \Gamma_p^h = \emptyset \text{ and} \\ &\Gamma_j^h \cap \Gamma_k^h \cap \partial\Omega = \emptyset \\ &\text{for } j \neq k,\ k \neq p,\ p \neq j. \end{aligned} \tag{42}$$

We stress that this "no cross-point" assumption enforces two conditions: three subdomains cannot be adjacent at any point *and* two subdomains cannot meet at the physical boundary $\partial\Omega$ of the computational domain. Examples of such geometric configurations are given in Figure 2 below.
We wish to study this situation, so we assume all through this section that (42) holds. Then, each interface is a closed manifold. In this case, we can introduce an operator $\mathrm{X} : \mathbb{V}_h(\Sigma) \to \mathbb{V}_h(\Sigma)$ consisting in swapping the traces from both sides of each interface

$$\mathfrak{v} = \mathrm{X}(\mathfrak{w}) \quad \Longleftrightarrow \quad \begin{cases} v_j = w_k & \text{on } \Gamma_j^h \cap \Gamma_k^h \qquad j \neq k, \\ v_j = w_j & \text{on } \Gamma_j^h \cap \partial\Omega \end{cases} \tag{43}$$

where $\mathfrak{v} = (v_1, \ldots, v_{\mathrm{J}})$, $\mathfrak{w} = (w_1, \ldots, w_{\mathrm{J}})$. This operator is widely spread in domain decomposition literature. It is in particular at the core of the Optimized Schwarz Methods (OSM), see [12, Formula (42)]. The next lemma (simple proof left to the reader) points a few elementary properties for this operator.

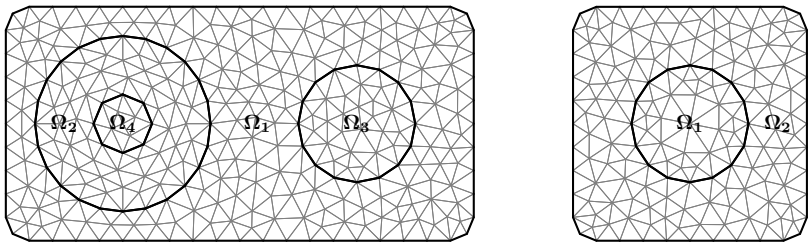

(a) (b)

Fig. 2: Examples of partitions without cross-point.

Lemma 12.1
If (42) *holds then the operator* X *defined by* (43) *maps continuously* $\mathbb{V}_h(\Sigma)$ *into* $\mathbb{V}_h(\Sigma)$. *Besides* $\mathrm{X}^2 = \mathrm{Id}$ *and* $(\mathrm{Id}+\mathrm{X})/2 : \mathbb{V}_h(\Sigma) \to \mathrm{V}_h(\Sigma)$ *is a projector onto the single-trace space* $\mathrm{V}_h(\Sigma)$.

There are striking similarities shared by both Π and X, see the definition of Π given by Lemma 6.2. Both operators coincide, if and only if $(\mathrm{Id}+\mathrm{X})/2$ is orthogonal for the scalar product $t_h(\cdot,\cdot)$, hence if and only if $(\mathrm{Id}+\mathrm{X})/2$ is self-adjoint for the scalar product $t_h(\cdot,\cdot)$ which writes equivalently

$$t_h(\mathrm{X}(\mathfrak{v}),\mathfrak{w}) = t_h(\mathfrak{v},\mathrm{X}(\mathfrak{w})) \quad \forall \mathfrak{v},\mathfrak{w} \in \mathbb{V}_h(\Sigma). \tag{44}$$

This condition is satisfied only under certain conditions on the impedance $t_h(\cdot,\cdot)$. The next result provides sufficient conditions for this: roughly speaking, the impedance operator should be "symmetric" with respect to all interfaces (except the physical boundary).

Proposition 12.2
Assume that the impedance t_h *is diagonal (cf Definition 5.6) and Condition* (42) *holds. Set* $\mathfrak{I} := \{(j,k) \in \{1,\dots,\mathrm{J}\}^2 : \ j<k \text{ and } \Gamma_j^h \cap \Gamma_k^h \neq \emptyset\}$ *and* $\Gamma_0^h := \partial\Omega$. *Then* $\mathrm{X} = \Pi$ *if there exist scalar products* $t_h^{j,k} : \mathrm{V}_h(\Gamma_j^h \cap \Gamma_k^h) \times \mathrm{V}_h(\Gamma_j^h \cap \Gamma_k^h) \to \mathbb{C}$ *such that*

$$t_h(\mathfrak{v},\mathfrak{w}) = \textstyle\sum_{k\in\{1,\dots,\mathrm{J}\}} t_h^{0,k}(v_k,w_k) + \sum_{(j,k)\in\mathfrak{I}} \big(t_h^{j,k}(v_j,w_j) + t_h^{j,k}(v_k,w_k) \big)$$
$$\forall\ \mathfrak{v} = (v_1,\dots,v_{\mathrm{J}}),\ \ \mathfrak{w} = (w_1,\dots,w_{\mathrm{J}}) \in \mathbb{V}_h(\Sigma).$$

Proof:
From (43), for $\mathfrak{v} = (v_1,\dots,v_{\mathrm{J}})$ and $\mathfrak{w} = (w_1,\dots,w_{\mathrm{J}})$ in $\mathbb{V}_h(\Sigma)$, we obtain the expression $t_h(\mathrm{X}(\mathfrak{v}),\mathfrak{w}) = \sum_{k\in\{1,\dots,\mathrm{J}\}} t_h^{0,k}(v_k,w_k) + \sum_{(j,k)\in\mathfrak{I}} [t_h^{j,k}(v_j,w_k) + t_h^{j,k}(v_k,w_j)]$. This proves (44) which, as previously discussed, shows that $\Pi = \mathrm{X}$. □

The previous result states that, when there is no cross-point and the impedance does not couple disjoint interfaces (which is actually a natural choice of impedance), then $\Pi = \mathrm{X}$. In this situation, Algorithm (29) appears to be a classical Optimized Schwarz Method: this is exactly the algorithm appearing for example in [16, §3.3], [14], [23, §5] or [32, chap.6].

This shows that (29) is a true generalization of OSM for the case where the subdomain partition contains cross-points.

Remark 12.3 *From the results of the present section, we deduce in particular that in the case of no cross-point and an impedance chosen according to Example 5.2, our method coincides with the original Després algorithm introduced in [16]. The theory from Section 9 and 10 then yields an estimate for the convergence rate of this algorithm, see* (41)*. To our knowledge, estimates of the convergence rate of Després algorithm had never been established in such a general setting.*

13 Matrix form of the algorithm

Coming back to the general situation where the subdomain partition may admit cross-points, in this section we will describe in more concrete terms the implementation of the iterative scheme (29), writing all equations in matrix form. This will help gaining a real insight on the implementation details underlying the solution strategy we propose.

First of all, we set a few matrix notations. We assume that the classical shape functions of $\mathbb{P}_k$-Lagrange finite elements are used, and we consider a numbering of the associated degrees of freedom in each subdomain and on each boundary: for $\Upsilon = \Omega_j^h$ or $\Upsilon = \Gamma_j^h$ for some $j = 1, \dots, \mathrm{J}$ we define

$$N(\Upsilon) := \mathrm{dim}\mathrm{V}_h(\Upsilon) \quad \text{and}$$
$$\mathrm{V}_h(\Upsilon) = \mathrm{span}_{k=1\dots N_\Upsilon}\{\varphi_k^\Upsilon\}.$$

Here the φ_k^Υ's refer to the usual $\mathbb{P}_k$-Lagrange shape functions associated to the triangulation in Υ. We assume that each shape function on Γ_j^h is obtained by taking the trace of some shape function on Ω_j^h. We also introduce local stiffness matrices $\mathbf{A}_j$ with size $N(\Omega_j^h) \times N(\Omega_j^h)$, local impedance matrices $\mathbf{T}_j$ with size $N(\Gamma_j^h) \times N(\Gamma_j^h)$, and local trace matrices $\mathbf{B}_j$ with size $N(\Gamma_j^h) \times N(\Omega_j^h)$. The entries of these matrices are defined by

$$(\mathbf{A}_j)_{k,l} := a_{\Omega_j^h}(\varphi_l^{\Omega_j^h}, \varphi_k^{\Omega_j^h}), \qquad \begin{cases} (\mathbf{B}_j)_{k,l} := 1 & \text{if } \varphi_k^{\Gamma_j^h} = \varphi_l^{\Omega_j^h}|_{\Gamma_j^h}, \\ (\mathbf{B}_j)_{k,l} := 0 & \text{otherwise.} \end{cases}$$
$$(\mathbf{T}_j)_{k,l} := t_h^j(\varphi_l^{\Gamma_j^h}, \varphi_k^{\Gamma_j^h}),$$

Finally we also set

$$N(\Sigma) := \mathrm{dim}\mathrm{V}_h(\Sigma).$$

For each degree of freedom $k = 1, \dots, N(\Sigma)$, set $s(k, j) = 0$ if k does not belong to Γ_j^h, and let $s(k, j)$ refer to the number of this degree of freedom local to Γ_j^h otherwise. The assumptions of conformity that we formulated on the triangulation (see Section 1 and 2) guarantee that we can find a basis of shape functions such that $\mathrm{V}_h(\Sigma) = \mathrm{span}_{k=1\dots N_\Sigma}\{\varphi_k^\Sigma\}$ where

$$\varphi_k^\Sigma = (\varphi_{s(k,1)}^{\Gamma_1^h}, \dots, \varphi_{s(k,\mathrm{J})}^{\Gamma_\mathrm{J}^h})$$
$$\text{setting } \varphi_0^{\Gamma_j^h} \equiv 0 \ \forall j.$$

To keep track of this, we introduce boolean matrices $\mathbf{Q}_j$ of size $N(\Gamma_j^h) \times N(\Sigma)$ defined by $(\mathbf{Q}_j)_{k,l} = 1$ if $k = s(l,j)$, and $(\mathbf{Q}_j)_{k,l} = 0$ otherwise. These matrices can be used to assemble $\mathbf{T}_\Sigma$ the Galerkin matrix of the impedance $t_h(\cdot,\cdot)$ restricted to $\mathrm{V}_h(\Sigma)$. It is of size $N(\Sigma) \times N(\Sigma)$ and admits the expression

$$(\mathbf{T}_\Sigma)_{k,l} := t_h(\varphi_k^\Sigma, \varphi_l^\Sigma)$$
$$\mathbf{T}_\Sigma = \mathbf{Q}_1^* \mathbf{T}_1 \mathbf{Q}_1 + \cdots + \mathbf{Q}_\mathrm{J}^* \mathbf{T}_\mathrm{J} \mathbf{Q}_\mathrm{J}.$$

Finally we also need to introduce local contributions of the right-hand side represented by vectors $\mathbf{f}_j$ of size $N(\Omega_j^h)$ defined by $(\mathbf{f}_j)_k := \ell_{\Omega_j^h}(\varphi_k^{\Omega_j^h})$. After assembly of the matrices introduced above, and a proper choice of the relaxation parameter r and maximum number of iterations $n_{\max}$, the iterative scheme (29) takes the form of Algorithm (1) below. The whole algorithm is then parallel except for the step appearing in Line 10 which ensures coupling between subdomains (see also Remark 6.3).

Algorithm 1

1: **for** $j = 1, \ldots, \mathrm{J}$ **do** ▷ Initialisation
2: $\quad \mathbf{p}_j = 0$ ▷ size: $N(\Gamma_j^h)$
3: $\quad \mathbf{u}_j = (\mathbf{A}_j - i\mathbf{B}_j^* \mathbf{T}_j \mathbf{B}_j)^{-1} \mathbf{f}_j$ ▷ Local solve (size: $N(\Omega_j^h)$)
4: **end for**
5: **for** $n = 1, \ldots, n_{\max}$ **do**
6: $\quad \mathbf{g} = 0$ ▷ size: $N(\Sigma)$
7: $\quad$ **for** $j = 1, \ldots, \mathrm{J}$ **do**
8: $\quad\quad \mathbf{g} = \mathbf{g} + \mathbf{Q}_j^* \mathbf{T}_j (\mathbf{p}_j + 2i\mathbf{B}_j \mathbf{u}_j)$ ▷ Local scattering
9: $\quad$ **end for**
10: $\quad \mathbf{v} = \mathbf{T}_\Sigma^{-1} \mathbf{g}$ ▷ Global exchange
11: $\quad$ **for** $j = 1, \ldots, \mathrm{J}$ **do**
12: $\quad\quad \mathbf{p}_j = \mathbf{p}_j + 2r(i\mathbf{B}_j \mathbf{u}_j - \mathbf{Q}_j \mathbf{v})$
13: $\quad\quad \mathbf{u}_j = (\mathbf{A}_j - i\mathbf{B}_j^* \mathbf{T}_j \mathbf{B}_j)^{-1} (\mathbf{B}_j^* \mathbf{T}_j \mathbf{p}_j + \mathbf{f}_j)$ ▷ Local solve (size: $N(\Omega_j^h)$)
14: $\quad$ **end for**
15: **end for**

While the theoretical analysis of the Richardson algorithm (29) allows to get some deep insight on the efficiency of the method, such an algorithm is rarely used in practice. Krylov methods are the preferred choice in real-life applications, in particular one will typically resort to the GMRes algorithm in our non-symmetric case. Importantly, (h-uniform) geometric convergence of the Richardson algorithm guarantees (h-uniform) geometric convergence of its GMRes counter-part, even the restarted version.

Although other choices are possible, we solve iteratively using GMRes the linear system given by (27) which features a multi-trace as unknown. To define the algorithm, it suffices to provide a definition for a right-hand-side and a matrix-vector product routine. The right-hand-side is a J-tuple $(\mathbf{b}_1, \ldots, \mathbf{b}_J)$ and can be computed (offline) according to Algorithm 2. The matrix-vector product procedure, which takes as input a J-tuple $(\mathbf{p}_1, \ldots, \mathbf{p}_J)$ and outputs a J-tuple $(\mathbf{q}_1, \ldots, \mathbf{q}_J)$, is given in Algorithm 3. Notice again here that apart from the computation in Line

7 of Algorithm 3 which ensures coupling between subdomains, all operations are local to the subdomains (see also Remark 6.3).

Algorithm 2

$\mathbf{g} = 0$ ▷ size: $N(\Sigma)$
for $j = 1, \ldots,$ J **do**
  $\mathbf{u}_j = (\mathbf{A}_j - i\mathbf{B}_j^*\mathbf{T}_j\mathbf{B}_j)^{-1}\mathbf{f}_j$ ▷ Local solve (size: $N(\Omega_j^h)$)
  $\mathbf{b}_j = 2i\,\mathbf{B}_j\mathbf{u}_j$ ▷ size: $N(\Gamma_j^h)$
  $\mathbf{g} = \mathbf{g} + 2i\,\mathbf{Q}_j^*\mathbf{T}_j\mathbf{B}_j\mathbf{u}_j$
end for
$\mathbf{v} = \mathbf{T}_\Sigma^{-1}\mathbf{g}$ ▷ Global exchange
for $j = 1, \ldots,$ J **do**
  $\mathbf{b}_j = \mathbf{b}_j - 2\,\mathbf{Q}_j\mathbf{v}$
end for

Algorithm 3

$\mathbf{g} = 0$ ▷ size: $N(\Sigma)$
for $j = 1, \ldots,$ J **do**
  $\mathbf{u}_j = (\mathbf{A}_j - i\mathbf{B}_j^*\mathbf{T}_j\mathbf{B}_j)^{-1}(\mathbf{B}_j^*\mathbf{T}_j\mathbf{p}_j)$ ▷ Local solve (size: $N(\Omega_j^h)$)
  $\mathbf{q}_j = -2i\,\mathbf{B}_j\mathbf{u}_j$ ▷ size: $N(\Gamma_j^h)$
  $\mathbf{g} = \mathbf{g} + \mathbf{Q}_j^*\mathbf{T}_j(\mathbf{p}_j + 2i\mathbf{B}_j\mathbf{u}_j)$ ▷ Local scattering
end for
$\mathbf{v} = \mathbf{T}_\Sigma^{-1}\mathbf{g}$ ▷ Global exchange
for $j = 1, \ldots,$ J **do**
  $\mathbf{q}_j = \mathbf{q}_j + 2\,\mathbf{Q}_j\mathbf{v}$
end for

14 Numerics

In this section, we report on a series of numerical results illustrating the theory of the previous sections. We emphasize that this section does not aim at evaluating the numerical performance of our method; this would require fine computational optimization for the evaluation of the exchange operator Π, which is beyond the scope of the present contribution. Discussing the computational cost induced by the exchange operator will be the subject of another forthcoming article. Our goal here is simply to exhibit numerical confirmation of our theory.

In all numerical experiments given below, we solve the model Problem (1) in a domain Ω which is either a disk in 2D or a ball in 3D. Unless stated otherwise, we consider $\mu \equiv 1$ and the wave number κ is uniform in the domain. The source terms are taken to be $f \equiv 0$ and $g = (\mu\partial_{\mathbf{n}} - i\kappa)u_{\text{inc}}$ where $u_{\text{inc}}(\boldsymbol{x}) = \exp(i\kappa\mathbf{d}\cdot\boldsymbol{x})$ with $\mathbf{d}$ the unit vector in the x direction.

We provide numerical results obtained for the Richardson algorithm (29) as well as results obtained with a restarted GMRES algorithm. In all our numerical experiments, the relaxation parameter of the Richardson algorithm is $r = 0.5$ and GMRES is restarted every 20 iterations. We provide various tables reporting the

number of iterations required to achieve a tolerance of 10^{-8} for the relative error defined at the iteration n as

$$(\text{relative error})^2 = \frac{\sum_{j=1\ldots \mathrm{J}} \|u^{(n)} - u^{(\infty)}\|^2_{\mathrm{H}^1(\Omega_j^h)}}{\sum_{j=1\ldots \mathrm{J}} \|u^{(0)} - u^{(\infty)}\|^2_{\mathrm{H}^1(\Omega_j^h)}}, \tag{45}$$

where $u^{(n)}$ is the volume solution at iteration n, $u^{(0)}$ is the initial volume solution (taken to be zero in practice) and $u^{(\infty)}$ is the exact discrete volume solution of the full (undecomposed) problem. The choice of this volume (energy) norm has the important benefit of being independent of the choice of impedance or mesh partition. Finally, we stress that the criterion for reaching convergence does not rely on the residual of the linear system that is solved. In all test runs that were performed, the convergence was stopped if a maximum number of 10^5 iterations was not enough to reach the set tolerance.

The impedance operators tested are: the Després impedance operator of Example 5.2, denoted by M with parameter $\kappa_R = \kappa$; the second order impedance operator of Example 5.3, denoted by K with parameters $a = \frac{1}{2\kappa}$ and $b = \kappa$; the (hypersingular) boundary integral operator given in Example 5.4, denoted by W with parameters $a = \kappa^2$ and $\delta = \frac{1}{\kappa}$; and the Schur complement based operator of Example 5.5, denoted by Λ.

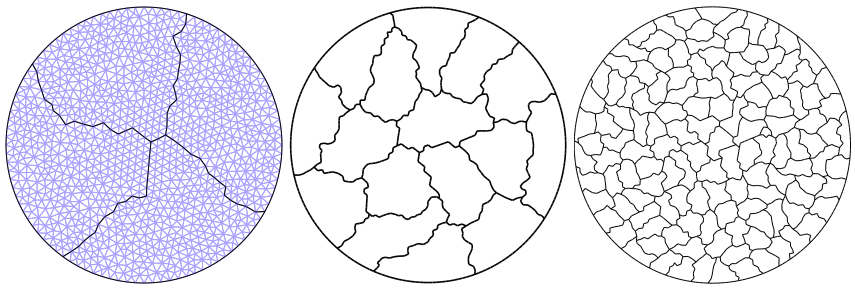

(a) J = 4. (b) J = 16. (c) J = 128.

Fig. 3: Examples of mesh partitions.

The research code that was used to run the tests was developed specifically to test the method and uses $\mathbb{P}_1$-Lagrange finite elements. It is written in Julia [3] and was validated on standard scattering test cases. The meshes are generated by Gmsh [26] and partitioned using Metis [31] through the Julia API. The integral operator matrices are computed thanks to the BemTool library[2], written in C++.

14.1 Influence of typical mesh size

We present a first test case consisting of a disk of radius $R = 1$ split roughly (using a mesh partitioner) in four quarters, see Figure 3a. The interest of this test case

[2] https://github.com/xclaeys/BemTool

is the presence of pure interior cross-points where three domains share a common vertex.

The full convergence history of the relative $\mathbb{H}^1$ error (45) for the Richardson and GMRES algorithms are provided for this test case in Figure 4 as an illustrative example of typical convergence.

We report the number of iterations to reach convergence with respect to mesh refinement in Figure 5 for the Richardson and GMRES algorithms. The refinement of the mesh is indicated by the number of points per wavelength $N_\lambda = 2\pi/(\kappa h)$ which is inversely proportional to the typical mesh size h. In Figure 5b we also report the number of GMRes iterations that are required to achieve the same error to solve the full (undecomposed) linear system (line plot labeled 'No DDM'). We see that this iteration count has a growth which is approximately quadratic with respect to N_λ, illustrating the deterioration of the matrix conditioning as the mesh is refined.

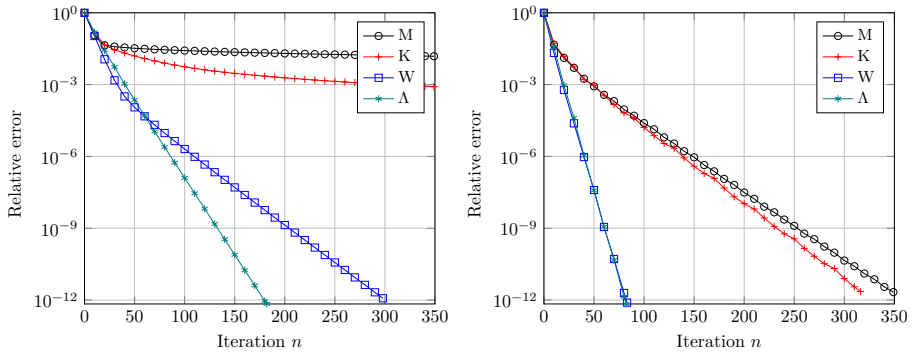

(a) Richardson algorithm (b) GMRES algorithm

Fig. 4: An example of convergence history. Fixed parameters $\kappa = 5$, J = 4, $N_\lambda = 2\pi/(\kappa h) = 40$, 2D, disk of radius $R = 1$.

For the local operators M and K the convergence is not uniform with respect to mesh refinement and a large number of iterations is required to reach the set tolerance. The growth of the iteration count appears to be quasi quadratic with respect to N_λ for the Richardson algorithm and quasi-linear for the GMRES algorithm. This agrees with the comments on the analytical estimates from Example 11.4 and Example 11.5 which therefore seem sharp. For small mesh size the convergence may not even be reached within 10^5 iterations. In contrast, the non-local operators W and Λ exhibit uniform convergence in all cases, with a very moderate number of iterations required to reach the set tolerance. This is also in agreement with the comments on the analytical estimates from Example 11.6 and Example 11.7.

We also provide some numerical results obtained in 3D. The domain Ω is now a ball of radius $R = 1$ partitioned into eight subdomains, which generate interior cross-point curves where three domains share common edges. Figure 6 reports the iteration count with respect to mesh refinement. Again in this case, we clearly

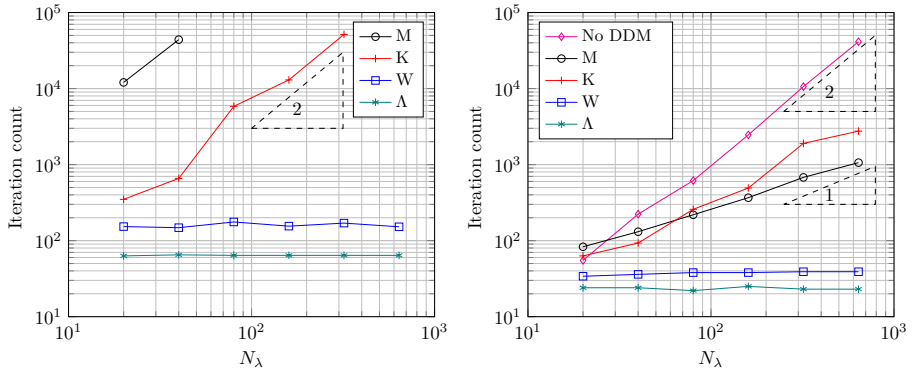

(a) Richardson algorithm (b) GMRes algorithm

Fig. 5: Number of iterations with respect to the number of mesh points per wavelength $N_\lambda = 2\pi/(\kappa h)$. Fixed parameters $\kappa = 1$, J = 4, 2D, disk of radius $R = 1$.

identify the non-uniformity of the convergence for the local operators M and K while the non-local operators W and Λ exhibit h-uniform convergence.

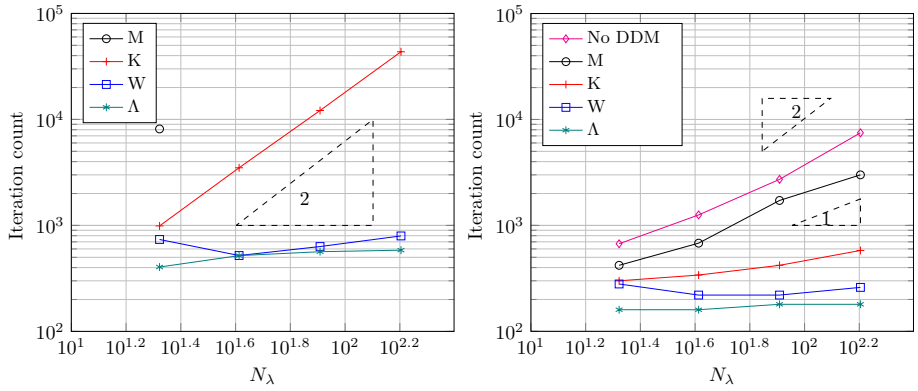

(a) Richardson algorithm (b) GMRes algorithm

Fig. 6: Number of iterations with respect to the number of mesh points per wavelength $N_\lambda = 2\pi/(\kappa h)$. Fixed parameters $\kappa = 1$, J = 8, 3D, sphere of radius $R = 1$.

14.2 Influence of the wave number

For the two-dimensional case, we now report the dependency of the iteration count with respect to the wave number κ, see Figure 7. To avoid pollution induced by phase error, the mesh width varies so as to maintain the relation $h^2\kappa^3 = (2\pi/20)^2$ i.e. $N_\lambda = 20$ points per wavelength at wave number $\kappa = 1$.

As the wave number κ increases, the discrete (as well as the continuous) problem becomes more difficult to solve. This is indicated again by the increase in the iteration count of the GMRes algorithm for the undecomposed problem (line plot labeled 'No DDM' in Figure 7b). On the other hand, for all the impedance operators under study, we notice a sub-linear growth of the number of iteration with respect to κ. The growth of iteration count is especially moderate for non-local impedances. Surprisingly, with W as impedance, the iteration count seems stable for Richardson's algorithm but not for GMRes. We have no explanation for this fact.

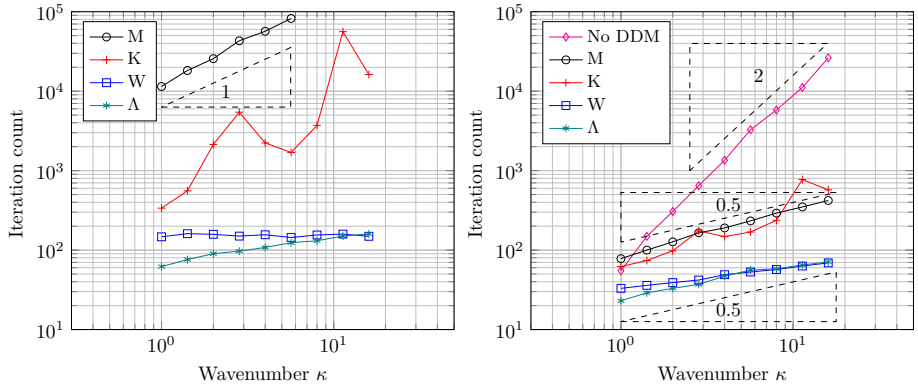

(a) Richardson algorithm (b) GMRes algorithm

Fig. 7: Number of iterations with respect to the wave number κ. Fixed parameters J = 4, $h^2\kappa^3 = (2\pi/20)^2$, 2D, disk of radius $R = 1$.

14.3 Influence of the number of subdomains

We finally study the dependency of the method with respect to the number of subdomains J of the mesh partition.

In the first set of results, we study the influence of the number of subdomains J on the iteration count for a problem with fixed size. Figure 8 reports the iteration count with respect to J varying from 2 to 1024 subdomains for a 2D configuration only. One can notice a sub-linear increase in the number of iterations to get to a converged solution. Notice that in this case the undecomposed linear system is kept the same. Hence, the fact that the discrete problem gets harder is a pure artificial effect of the DDM. Interestingly, we see that the number of iterations levels out for the coercive DtN operator, in a regime where the size of the sub-problems gets really small compared to the wavelength of the problem.

In the second set of results, the domain Ω increases in size as the number of subdomains J grows so as to keep a fixed number of degrees of freedom per subdomain. Figure 9 reports the iteration count with respect to J for the 2D

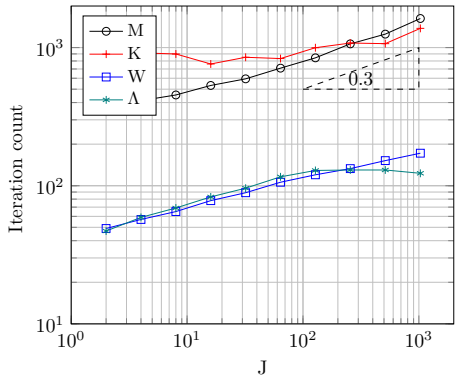

Fig. 8: Number of iterations with respect to the number of subdomains J for a fixed size problem. Fixed parameters $\kappa = 2$, $N_\lambda = 100$, 2D, disk of radius $R = 4$. GMRES algorithm.

and 3D cases. The size of the domain is chosen to grow like $\mathrm{J}^{1/d}$ where d is the dimension of ambient space, so as to keep a fixed size (in terms of DOFs) for the local subdomains. In 2D the domain is a disk of radius increasing from $R = 1$ to $R = 16$, and in 3D the domain is a sphere of radius increasing from $R = 1$ to $R = 3.7$. The growth of the number of iteration to reach the set tolerance also appears to scale like $\mathrm{J}^{1/d}$.

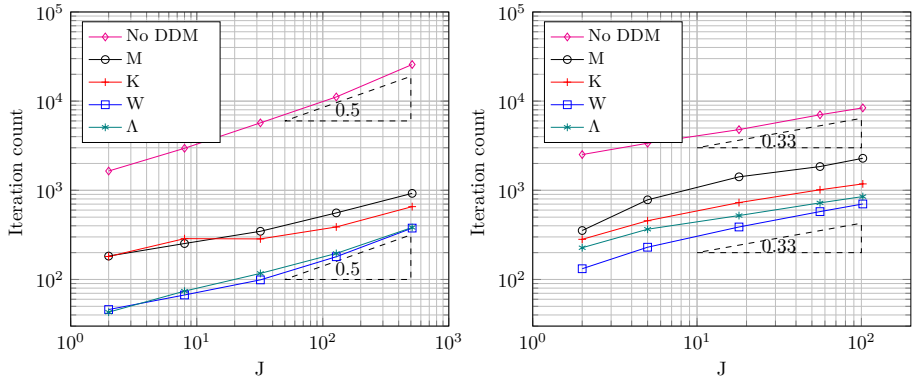

(a) Fixed parameters $\kappa = 5$, $N_\lambda = 40$, 2D (b) Fixed parameters $\kappa = 2$, $N_\lambda = 30$, 3D

Fig. 9: Number of iterations with respect to the number of subdomains J for a domain size growing like $\mathrm{J}^{1/d}$. Disk (left) and sphere (right) of increasing radius. GMRES algorithm.

14.4 Heterogeneous medium

We close the numerical experiment section with results in heterogeneous medium in 2D. The domain of propagation Ω is still a disk of radius $R = 1$, but this time with a circular inclusion of a different medium in the region with radius $R \leq 0.5$. The coefficient μ is still equal to 1 outside the inclusion and takes the value $\mu = 1 + \mu_r$ inside, with μ_r varying from 0 (homogeneous medium) to 4. Figure 10 reports the iteration counts for the GMRES algorithm as the medium varies. The partition is composed of 10 subdomains so that some interfaces are cut by the discontinuity in the medium. One can observe that the number of iterations to get to convergence increases greatly for the undecomposed problem (line plot labeled 'No DDM'). This is due to the appearance in the solution of "quasi-modes" of the inclusion with large amplitude. For an illustration of this effect, the modulus of the total field is represented in Figure 11 for the value $\mu_r = 4$. On the other hand, the DD algorithm performs well, with a number of iterations only mildly growing.

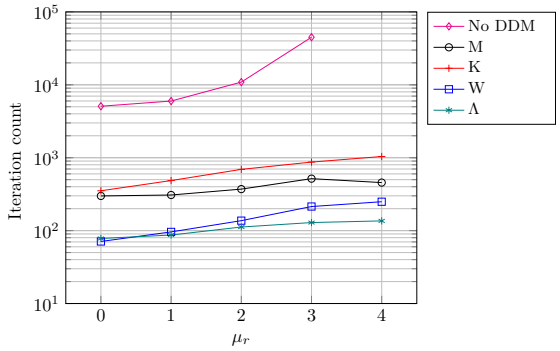

Fig. 10: Number of iterations with respect to increasing contrast in μ. Fixed parameters $\kappa = 10$, J $= 10$, $N_\lambda = 50$, 2D, disk of radius $R = 1$. GMRES algorithm.

Acknowledgments

This work was supported by the project NonlocalDD funded by the French National Research Agency, grant ANR–15–CE23–0017–01. The authors would like to thank Patrick Joly and Francis Collino for many inspiring discussions and, in particular, for pointing a simplification in the proof of Corollary 8.4.

References

1. Bendali, A., Boubendir, Y.: Dealing with cross-points in a non-overlapping domain decomposition solution of the helmholtz equation. In: G. Cohen, P. Joly, E. Heikkola, P. Neittaanmäki (eds.) Mathematical and Numerical Aspects of Wave Propagation WAVES 2003:

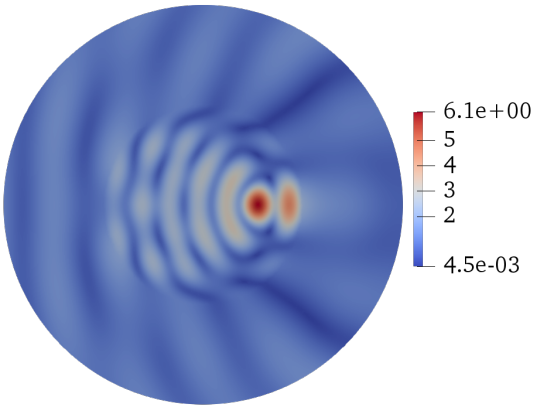

Fig. 11: Modulus of the total field. Fixed parameters $\kappa = 10$, $N_\lambda = 50$, 2D, disk of radius $R = 1$, $\mu_r = 4$.

Proceedings of The Sixth International Conference on Mathematical and Numerical Aspects of Wave Propagation, pp. 319–324 (2003)
2. Bendali, A., Boubendir, Y.: Non-overlapping domain decomposition method for a nodal finite element method. Numerische Mathematik **103**(4), 515–537 (2006)
3. Bezanson, J., Edelman, A., Karpinski, S., Shah, V.: Julia: A fresh approach to numerical computing. SIAM review **59**(1), 65–98 (2017)
4. Boubendir, Y., Antoine, X., Geuzaine, C.: A Quasi-Optimal Non-Overlapping Domain Decomposition Algorithm for the Helmholtz Equation. J. Comp. Phys. **213**(2), 262–280 (2012)
5. Brenner, S., Scott, L.: The mathematical theory of finite element methods. 3rd ed., vol. 15, 3rd ed. edn. New York, NY: Springer (2008)
6. Claeys, X.: A single trace integral formulation of the second kind for acoustic scattering. Tech. Rep. 14, Seminar for Applied Mathematics, ETH Zürich, Switzerland (2011)
7. Claeys, X.: Quasi-local multitrace boundary integral formulations. Numer. Methods Partial Differential Equations **31**(6), 2043–2062 (2015)
8. Claeys, X.: Non-local variant of the optimised Schwarz method for arbitrary non-overlapping subdomain partitions. ESAIM Math. Model. Numer. Anal. **55**(2), 429–448 (2021)
9. Claeys, X., Collino, F., Joly, P., Parolin, E.: A discrete domain decomposition method for acoustics with uniform exponential rate of convergence using non-local impedance operators. In: Domain Decomposition Methods in Science and Engineering XXV. Springer International Publishing (2019)
10. Claeys, X., Hiptmair, R.: Multi-trace boundary integral formulation for acoustic scattering by composite structures. Comm. Pure Appl. Math. **66**(8), 1163–1201 (2013)
11. Claeys, X., Thierry, B., Collino, F.: Integral equation based optimized Schwarz method for electromagnetics. In: Domain decomposition methods in science and engineering XXIV, *Lect. Notes Comput. Sci. Eng.*, vol. 125, pp. 187–194. Springer, Cham (2018)
12. Collino, F., Ghanemi, S., Joly, P.: Domain decomposition method for harmonic wave propagation: a general presentation. Computer Methods in Applied Mechanics and Engineering **184**(2), 171 – 211 (2000)
13. Collino, F., Joly, P., Lecouvez, M.: Exponentially convergent non overlapping domain decomposition methods for the helmholtz equation. ESAIM M2AN (2019). Accepted
14. Després, B.: Décomposition de domaine et problème de Helmholtz. C. R. Acad. Sci. Paris Sér. I Math. **311**(6), 313–316 (1990)
15. Després, B.: Domain decomposition method and the Helmholtz problem. In: Mathematical and numerical aspects of wave propagation phenomena (Strasbourg, 1991), pp. 44–52. SIAM, Philadelphia, PA (1991)

16. Després, B.: Méthodes de décomposition de domaine pour les problèmes de propagation d'ondes en régime harmonique. Le théorème de Borg pour l'équation de Hill vectorielle. Institut National de Recherche en Informatique et en Automatique (INRIA), Rocquencourt (1991). Thèse, Université de Paris IX (Dauphine), Paris, 1991
17. Després, B.: Domain decomposition method and the Helmholtz problem. II. In: Second International Conference on Mathematical and Numerical Aspects of Wave Propagation (Newark, DE, 1993), pp. 197–206. SIAM, Philadelphia, PA (1993)
18. Després, B., Nicolopoulos, A., Thierry, B.: Corners and stable optimized domain decomposition methods for the Helmholtz problem (2020). Preprint available on HAL ref. hal-02612368.
19. Dolean, V., Jolivet, P., Nataf, F.: An introduction to domain decomposition methods. Society for Industrial and Applied Mathematics (SIAM), Philadelphia, PA (2015). Algorithms, theory, and parallel implementation
20. El Bouajaji, M., Thierry, B., Antoine, X., Geuzaine, C.: A quasi-optimal domain decomposition algorithm for the time-harmonic maxwell's equations. Journal of Computational Physics **294**, 38–57 (2015)
21. Ern, A., Guermond, J.: Theory and Practice of Finite Elements. Applied Mathematical Sciences. Springer New York (2004)
22. Gander, M., Kwok, F.: On the applicability of Lions' energy estimates in the analysis of discrete optimized schwarz methods with cross points. Lecture Notes in Computational Science and Engineering **91** (2013)
23. Gander, M., Magoulès, F., Nataf, F.: Optimized Schwarz methods without overlap for the Helmholtz equation. SIAM J. Sci. Comput. **24**(1), 38–60 (2002)
24. Gander, M., Santugini, K.: Cross-points in domain decomposition methods with a finite element discretization. Electron. Trans. Numer. Anal. **45**, 219–240 (2016)
25. Gander, M., Xu, Y.: Optimized Schwarz methods for model problems with continuously variable coefficients. SIAM J. Sci. Comput. **38**(5), A2964–A2986 (2016)
26. Geuzaine, C., Remacle, J.F.: Gmsh: A 3-d finite element mesh generator with built-in pre- and post-processing facilities. International Journal for Numerical Methods in Engineering **79**, 1309 – 1331 (2009)
27. Graham, I., Spence, E., Zou, J.: Domain decomposition with local impedance conditions for the Helmholtz equation with absorption. SIAM J. Numer. Anal. **58**(5), 2515–2543 (2020)
28. Graham, I.G., Sauter, S.A.: Stability and finite element error analysis for the Helmholtz equation with variable coefficients. Math. Comput. **89**(321), 105–138 (2020)
29. Grisvard, P.: Elliptic problems in nonsmooth domains. Reprint of the 1985 hardback ed, vol. 69, reprint of the 1985 hardback ed. edn. Philadelphia, PA: Society for Industrial and Applied Mathematics (SIAM) (2011)
30. Ihlenburg, F.: Finite element analysis of acoustic scattering, *Applied Mathematical Sciences*, vol. 132. Springer-Verlag, New York (1998)
31. Karypis, G., Kumar, V.: A fast and high quality schema for partitioning irregular graphs. Siam Journal on Scientific Computing **20** (1999)
32. Lecouvez, M.: Iterative methods for domain decomposition without overlap with exponential convergence for the Helmholtz equation. Theses, Ecole Polytechnique (2015)
33. Loisel, S.: Condition number estimates for the nonoverlapping optimized schwarz method and the 2-lagrange multiplier method for general domains and cross points. SIAM Journal on Numerical Analysis **51**(6), 3062–3083 (2013)
34. Magoulès, F., Iványi, P., Topping, B.H.V.: Non-overlapping Schwarz methods with optimized transmission conditions for the Helmholtz equation. Comput. Methods Appl. Mech. Engrg. **193**(45–47), 4797–4818 (2004)
35. Melenk, J.M., Sauter, S.: Wavenumber explicit convergence analysis for Galerkin discretizations of the Helmholtz equation. SIAM J. Numer. Anal. **49**(3), 1210–1243 (2011)
36. Modave, A., Royer, A., Antoine, X., Geuzaine, C.: An optimized Schwarz domain decomposition method with cross-point treatment for time-harmonic acoustic scattering (2020). Working paper or preprint
37. Pechstein, C.: Finite and boundary element tearing and interconnecting solvers for multiscale problems, *Lecture Notes in Computational Science and Engineering*, vol. 90. Springer, Heidelberg (2013)
38. Sauter, S., Schwab, C.: Boundary element methods, *Springer Series in Computational Mathematics*, vol. 39. Springer-Verlag, Berlin (2011). Translated and expanded from the 2004 German original

39. Scott, L., Zhang, S.: Finite element interpolation of nonsmooth functions satisfying boundary conditions. Math. Comput. **54**(190), 483–493 (1990)
40. Spillane, N., Rixen, D.J.: Automatic spectral coarse spaces for robust finite element tearing and interconnecting and balanced domain decomposition algorithms. Int. J. Numer. Methods Eng. **95**(11), 953–990 (2013)
41. St-Cyr, A., Rosenberg, D., Kim, S.D.: Optimized schwarz preconditioning for sem based magnetohydrodynamics. In: M. Bercovier, M.J. Gander, R. Kornhuber, O. Widlund (eds.) Domain Decomposition Methods in Science and Engineering XVIII, pp. 209–216 (2009)
42. Steinbach, O.: Numerical approximation methods for elliptic boundary value problems. Springer, New York (2008). Finite and boundary elements, Translated from the 2003 German original
43. Toselli, A., Widlund, O.: Domain decomposition methods—algorithms and theory, *Springer Series in Computational Mathematics*, vol. 34. Springer-Verlag, Berlin (2005)